Effects of Resonant Cavity on Macroscopic Quantum Tunneling of Fluxon in Long Josephson Junctions

Ju H. Kim and Ramesh P. Dhungana*
Department of Physics and Astrophysics, University of North Dakota, Grand Forks, ND 58202-7129

We investigate the effects of high-Q_c resonant cavity on macroscopic quantum tunneling (MQT) of fluxon both from a metastable state to continuum and from one degenerate ground-state of a double-well potential to the other. By using a set of two coupled perturbed sine-Gordon equations, we describe the tunneling processes in linear long Josephson junctions (LJJs) and find that MQT in the resonant cavity increases due to potential renomalization, induced by the interaction between the fluxon and cavity. Enhancement of the MQT rate in the weak-coupling regime is estimated by using the experimantally accessible range of the model parameters. The tunneling rate from the metastable state is found to increase weakly with increasing junction-cavity interaction strength. However, the energy splitting between the two degenerate ground-states of the double-well potential increases significantly with increasing both the interaction strength and frequency of the resonant cavity mode. Finally, we discuss how the resonant cavity may be used to tune the property of Josephson vortex quantum bits.

PACS numbers: 74.50.+r, 74.78.Na, 85.25.Cp

I. INTRODUCTION

Experimentally observed[2] quantum behavior of Josephson vortices (i.e., fluxons) at ultra-low temperatures has opened up a possibility of realizing quantum computers based on long Josephson junctions (LJJs). This observation led to much interest on Josephson vortex quantum bit[3–5] (qubit) as an alternative to the previously proposed superconducting qubits. Similar to other approaches based on Josephson junctions such as charge,[6] phase,[7] and flux[8] qubits, Josephson vortex qubit (JVQ) is also a promising candidate for quantum computation application. Due to its weak interaction with decoherence sources in the environment at low temperatures, the JVQ may have significant advantages over the other superconducting qubits. For instance, a significantly longer decoherence time was suggested as one such advantage.[4]

The JVQ takes advantage of the coherent superposition of two spatially separated states arising from the low temperture property of a trapped fluxon in a double-well potential. This property includes (i) energy quantization and (ii) macroscopic quantum tunneling[2](MQT). We note that, for linear LJJs, the fluxon potential for either metastable state or JVQ may be obtained[9] by using Nb-AlO_x-Nb junctions and by implanting either one or two microresistors in the insulator layer, respectively. For application of JVQs, tuning both the decoherence time and the level of entaglement by controlling the qubit property is essential. However, due to its weak interaction with external perturbations, an effective tuning mechanism for JVQ is less clear. Recent studies[10,11] on using microwave cavity for both tuning a single phase qubit and inducing interaction between either two charge or two phase qubits suggest that resonant cavity may be used for JVQ to serve the same purpose.

Earlier studies on the effects of resonant cavity indicate[12,13] that both electric and magnetic fields of the cavity couple to the Josephson junction since the cavity electromagnetic (EM) mode behaves similar to a phonon mode[14] which interacts with the fluxon. The effects of resonant cavity on the fluxon dynamics in LJJ stacks[15–17] have been studied both experimentally[18,19] and theoretically.[20–22] These studies show that when the coupling between LJJ and resonant cavity is spatially uniform, no force is exerted on the fluxon by the cavity, but its dynamics may become modified. These studies suggest that the interaction between LJJ and a resonant EM wave mode of the cavity promotes[23] collective dynamics of fluxons. The in-phase locking mode of the fluxon dynamics is shown to be enhanced[23] by the cavity EM mode.

These studies also suggest that the junction-cavity interaction may be used to change the qubit property. The property of JVQ depends on MQT between two spatially separated states of the fluxon. We note that MQT represents quantum particle-like collective exciations.[24,25] As semi-classical theories indicate that the MQT rate[26] depends on the potential barrier height, the JVQ can be tuned by adjusting the potential-well for the fluxon. This adjustment can be achieved by potential renormalization induced by the junction-cavity interaction since this interaction can strongly affect the fluxon tunneling processes, similar to phonon assisted tunneling in Josephson junctions.[27] We note that a two-level atom interacting with a quantized radiation field, described by the Jaynes-Cummings model,[28] is also similar to the JVQ-cavity system that we consider in the present work. The potential renormalization for fluxon suggests that the resonant cavity may be used as a tool for controlling the JVQ property. As the fluxon tunneling processes may be controlled externally by tuning either the junction-cavity coupling strength or the resonant frequency, the effects of the resonant cavity depend on the nature of the interaction. However, the influence of junction-cavity interaction on

the MQT rate has not been understood clearly.

In this paper, we investigate the effects of the junction-cavity both on MQT from metastable state and on the ground-state energy splitting in a double-well potential. We note that, to focus on the interaction between LJJ and a single resonant cavity mode, we consider only a high-Q_c cavity. First, we estimate the MQT rate for the fluxon in a single LJJ and for the phase-locked fluxons in a coupled LJJ stack by computing the local and non-local contributions. Then, we estimate the effects of resonant cavity on the JVQ property by computing the ground-state energy splitting. Before proceeding further, we outline the main result. (i) *The potential barrier for a fluxon in the metastable state is not affected by increasing neither the junction-cavity interaction nor the resonant frequency of the cavity EM mode.* (ii) *The non-local contribution to the tunneling rate due to the junction-cavity interaction is negligible in the weak-coupling regime.* (iii) *Due to potential renormalization induced by the junction-cavity interaction, the potenital barrier height for the fluxon trapped in a double-well potential is reduced. This reduction leads to increase in the ground-state energy splitting for the JVQ with increasing junction-cavity coupling and resonant frequency.*

The outline of the remainder of the paper is as follows. In Sec. II, we describe the LJJ-cavity system by using a set of two perturbed sine-Gordon equations. In Sec. III, the effects of resonant cavity on the fluxon tunneling rate from the metastable state in a LJJ are discussed. In Sec. IV, we discuss MQT of phase-locked fluxons from the metastable state in a vertical stack of two coupled LJJs. In Sec. V, the effects of interaction between LJJ and a single mode in high-Q_c cavity on JVQ are estimated by computing the ground-state energy splitting. Finally, we summarize the result and conclude in Sec. VI.

II. COUPLED LONG JOSEPHSON JUNCTIONS IN RESONANT CAVITY

To examine i) one-fluxon tunneling in a single LJJ, ii) phase-locked two-fluxon tunneling in a stack of two coupled LJJs, and iii) the ground-state energy splitting in JVQ, we start with coupled perturbed sine-Gordon equations[15] for describing two LJJs which interact with resonant cavity[13]

$$\frac{\partial^2}{\partial x^2}\Big(\varphi_1 - \mathcal{S}\varphi_2\Big) - \frac{\partial^2\varphi_1}{\partial t^2} - \sin\varphi_1 = \mathcal{F}_1 \tag{1}$$

$$\frac{\partial^2}{\partial x^2}\Big(\varphi_2 - \mathcal{S}\varphi_1\Big) - \frac{\partial^2\varphi_2}{\partial t^2} - \sin\varphi_2 = \mathcal{F}_2 \tag{2}$$

where x and t are the dimensionless coordinates in units of $\lambda_J\gamma^{-1}(\mathcal{S})$ and ω_p^{-1}, respectively. Here $\gamma^{-1}(\mathcal{S}) = \sqrt{1-\mathcal{S}^2}$ and ω_p denotes the plasma frequency. The dynamic variable φ_i represents the difference between the phase ϕ of the superconductor order parameter for the two superconductor (S) layers i and $i-1$ (i.e., $\varphi_i = \phi_i - \phi_{i-1}$). The strength of magnetic induction coupling between two LJJs is denoted by $\mathcal{S}$. Here we set $\hbar = k_B = c = 1$ for convenience. The perturbation term $\mathcal{F}$ of for each LJJ which is given by

$$\mathcal{F}_i = \beta\frac{\partial\varphi_i}{\partial t} + f_i - g_E\frac{d^2q_r}{dt^2} - \epsilon_i\delta(x-x_i^o)\sin\varphi_i \tag{3}$$

accounts for the contribution from dissipation (β), bias current ($f = J^B/J_c$), resonant cavity (g_E), and microresistors ($\epsilon = (J_c - J_c')l_b/J_c\lambda_J$). Here x_i^o, J^B, J_c, J_c', l_b ($\ll \lambda_J$) and λ_J denote the position of microresistors in the insulator layer of the i-th junction, the bias current density, the critical current density, the modified current density, the length of the LJJ in which J_c is modified, and the Josephson length, respectively. We note that dissipation, bias currents, resonant cavity and microresistors on the phase dynamics lead to different effects.

We account for the perturbation contribution due to resonant cavity by following Tornes and Stroud[13] and by assuming that the cavity supports a single harmonic oscillator mode which may be represented by the *displacement* variable q_r as

$$\frac{d^2q_r}{dt^2} + \frac{\omega_r}{Q_c}\frac{dq_r}{dt} + \omega_r^2 q_r = \frac{g_E\gamma(\mathcal{S})}{M_{osc}}\int dx\frac{\partial^2}{\partial t^2}\Big(\varphi_1+\varphi_2\Big). \tag{4}$$

Here ω_r, Q_c, and M_{osc} are the dimensionless oscillator frequency in units of ω_p, the cavity quality factor, and the "mass" of the oscillator mode, respectively. For simplicity, *we neglect the second term on the left hand side of Eq. (4) by assuming that the cavity is non-dissipative (i.e., high-Q_c cavity).* Also, we assume that the cavity electric field $\mathbf{E}$ is uniform within the junction by considering the spatially uniform junction-cavity coupling g_E of

$$g_E = -\frac{\epsilon_d}{2e}\sqrt{\frac{M_{osc}}{4\pi}}\ \mathbf{E}\cdot\hat{\mathbf{z}}, \tag{5}$$

where ϵ_d is the dielectric constant. As we will discuss below, the position independent coupling g_E does not change the fluxon motion directly but yields potential renormalization when a microresistor is present.

To estimate the effects of interaction between LJJ and resonant cavity analytically, we consider the weak perturbation $\mathcal{F}$ limit. As each perturbation term in Eq. (3) is small and does not change the form of the kink solution within the lowest order approximation,[29] we describe the fluxon motion in terms of the center coordinate $q(t)$. In the absence of both the perturbation terms ($\mathcal{F} = 0$) and the magnetic induction effect ($\mathcal{S} = 0$), the fluxon solution to Eq. (1) is given by

$$\varphi_i(x,t) \approx 4\tan^{-1}\Big[e^{\gamma(v_i)[x-q_i(t)]}\Big]\ , \tag{6}$$

in the non-relativistic limit (i.e., $v \ll 1$). Here $q_i(t) = v_i t$ denotes the center coordinate for the fluxon, and v is the fluxon speed in units of Swihart velocity. Equation (6)

represents propagation of nonlinear wave as a ballistic particle. The perturbation contributions of $\mathcal{F}$ only affect the dynamics of fluxon expressed in the q coordinate.

We now describe the fluxon phase dynamics in the coupled LJJ using the center coordinate q_i representation. The energy of the fluxon may be seen easily from the Euclidean Lagrangian (i.e., $\tau = it$),

$$\mathcal{L} = \mathcal{L}_o + \mathcal{L}_{mag} + \mathcal{L}_{pert} + \mathcal{L}_{osc} + \mathcal{L}_{coup} \ . \tag{7}$$

The first three terms for $\mathcal{L}$ of Eq. (7) describe the LJJ contributions, while the remaining two terms arise from the resonant cavity. First, we discuss the LJJ contributions to Lagrangian $\mathcal{L}$. The unperturbed part of LJJ is described by the Lagrangian $\mathcal{L}_o$ given by

$$\mathcal{L}_o = \sum_i \int \frac{dx}{2}\left[\left(\frac{\partial\varphi_i}{\partial\tau}\right)^2 + \left(\frac{\partial\varphi_i}{\partial x}\right)^2 + 2(1-\cos\varphi_i)\right] . \tag{8}$$

The Lagrangian contribution from the magnetic induction effect, $\mathcal{L}_{mag}$, is given by

$$\mathcal{L}_{mag} = \mathcal{S}\int dx \left(\frac{\partial\varphi_1}{\partial x}\right)\left(\frac{\partial\varphi_2}{\partial x}\right) \ . \tag{9}$$

We note that $\mathcal{L}_{mag}$ accounts for the interaction energy E_{int} between two LJJs due to the magnetic induction effect. The perturbation contribution to the Lagrangian, $\mathcal{L}_{pert} = \mathcal{L}_{nd} + \mathcal{L}_d$, is expressed as the sum of two terms: i) the non-dissipative ($\mathcal{L}_{nd}$) and ii) dissipative ($\mathcal{L}_d$) part. The non-dissipative contribution comes from the bias currents and microresistors. The non-dissipative Lagrangian $\mathcal{L}_{nd}$ is expressed as the sum of the contributions from the bias current ($\mathcal{L}_{bias}$) and microresistors ($\mathcal{L}_{pin}$) (i.e., $\mathcal{L}_{nd} = \mathcal{L}_{bias} + \mathcal{L}_{pin}$). The bias current contribution $\mathcal{L}_{bias}$ is given by

$$\mathcal{L}_{bias} = \sum_i \int dx f_i\varphi_i \ , \tag{10}$$

and the inhomogeneity contribution due to microresistors $\mathcal{L}_{pin}$ is given by

$$\mathcal{L}_{pin} = \sum_i \int dx \ \epsilon_i\delta(x - x_i^o)(1-\cos\varphi_i) \ . \tag{11}$$

We note that $\mathcal{L}_{pin}$ accounts for the fluxon pinning energy E_{pin}. These non-dissipative contributions provide the bare fluxon potential $V(q)$. On the other hand, the dissipative Lagrangian $\mathcal{L}_d$ accounts for the interaction between the fluxon and environment. The effects of this contribution may be described[30] by following Caldeira and Leggett and by representing the environment as a heat bath. The heat bath is represented as harmonic oscillators with generalized momenta P_i and coordinates Q_i. The dissipation Lagrangian $\mathcal{L}_d$ which accounts for the coupling between the phase (φ) and oscillator (Q_i) variables is given by

$$\mathcal{L}_d = \int dx \sum_i \left[\frac{P_i^2}{2m_i} + \frac{m_i\omega_i^2}{2}\left(Q_i - \frac{c_i\varphi}{m_i\omega_i^2}\right)^2\right] \ . \tag{12}$$

Here, the spectral function $J_\beta(\omega)$,

$$J_\beta(\omega) = \frac{\pi}{2}\sum_i \frac{c_i^2}{m_i\omega_i^2}\ \delta(\omega-\omega_i) = \beta\omega, \tag{13}$$

is used to reproduce the dissipation effects (β) in Eq. (3). The effects of dissipation on a two-state system has been studied extensively by using the spin-boson model.[31] In the adiabatic approximation, the energy splitting for the two-state system is known to be reduced[31] in the dissipative environment. However, this result does not[30] imply that the effects of the interaction between the two-state system and a single oscillator, which represents either a phonon or quantized radiation field, on the energy spliting is similar. In our discussion below, we neglect the dissipation effects by setting $\beta = 0$ since these effects are small at low temperatures, and we focus on the effects due to a resonant cavity.

We now discuss the high-Q_c resonant cavity contribution to the Lagrangian $\mathcal{L}$ of Eq. (7). The resonant cavity is modeled by using Lagrangian for a single harmonic oscillator which represents a single EM-mode supported by the cavity. The Lagrangian for this single mode oscillator $\mathcal{L}_{osc}$ is written as

$$\mathcal{L}_{osc} = \frac{M_{osc}}{2}\left(\frac{dq_r}{d\tau}\right)^2 + \frac{K}{2}\ q_r^2, \tag{14}$$

where K is the "spring constant" and q_r denotes the oscillator coordinate. We note that the oscillator frequency ω_r in Eq. (4) is given by $\omega_r = (K/M_{osc})^{1/2}$. The capacitive coupling between LJJ and resonant cavity is described by the Lagrangian $\mathcal{L}_{coup}$ as

$$\mathcal{L}_{coup} = -g_E\left(\frac{dq_r}{d\tau}\right)\ \int dx\ \sum_i\left(\frac{\partial\varphi_i}{\partial\tau}\right) . \tag{15}$$

Here we assume that the coordinate q_r is spatially homogeneous and focus on the effects of the uniform **E**-field in the cavity. We note that the interaction between LJJ and resonant cavity yields the non-local effects, similar to those from the dissipation term (i.e., $\beta \neq 0$).

We estimate MQT of fluxon by using the usual semiclassical approach[32] of starting with the partition function $\mathcal{Z}$ for the junction-cavity system

$$\mathcal{Z} = \int \mathcal{D}[\varphi]\mathcal{D}[q_r]\exp\{-S[\varphi, q_r]\} \tag{16}$$

where $S[\varphi, q_r] = \int d\tau\mathcal{L}$ is the action and $\mathcal{L}$ is the Lagrangian of Eq. (7). By noting that shape distortion of the fluxon due to weak perturbation (i.e., small $\mathcal{F}$) is negligible, we may rewrite the partition function $\mathcal{Z}$ in terms of $q(\tau)$ and $q_r(\tau)$ as

$$\mathcal{Z} = \int \mathcal{D}[q]\int \mathcal{D}[q_r]e^{-S[q,q_r]} \ . \tag{17}$$

Also by noting that the Lagrangian $\mathcal{L}_{coup}$ of Eq. (15) which accounts for the interaction between LJJ and

resonant cavity is linear in both coordinates q_r and φ, we separate the partition function $\mathcal{Z}$ into the resonant cavity and fluxon contribution by expressing $\mathcal{Z} = \mathcal{Z}_{res}\mathcal{Z}_{fluxon}$. The resonant cavity ($\mathcal{Z}_{res}$) and fluxon ($\mathcal{Z}_{fluxon}$) contribution to $\mathcal{Z}$ are given, respectively, as $\mathcal{Z}_{res} = \int \mathcal{D}[q_r(\omega_n)] \exp\{-S_{res}[q_r(\omega_n)]\}$ and $\mathcal{Z}_{fluxon} = \int \mathcal{D}[q(\tau)] \exp\{-S_{eff}[q(\tau)]\}$. The action for the resonant cavity contribution $S_{res}[q_r]$ is given by

$$S_{res}[q_r] = T\sum_{\omega_n} \frac{M_{osc}}{2}\left(\omega_n^2+\omega_r^2\right) \times \left[q_{r,n} + \frac{2\pi g_E q_n \omega_n^2}{M_{osc}(\omega_n^2+\omega_r^2)}\right]\left[q_{r,-n} + \frac{2\pi g_E q_{-n}\omega_n^2}{M_{osc}(\omega_n^2+\omega_r^2)}\right] \quad (18)$$

where $q_{r,n} = q_r(\omega_n)$, $q_n = q(\omega_n)$, $\omega_n = 2\pi nT$ is the Matsubara frequency, and T is the temperature. The action for the fluxon contribution $S_{eff}[q]$ is given by

$$S_{eff}[q] = \int d\tau \left[\frac{M_e}{2}\sum_{i=1}^{2}\dot{q}_i^2 + V(q) + \frac{\bar{g}_E^2\omega_r^2}{1-\mathcal{S}^2}(\sum_{i=1}^{2} q_i)^2\right] - \frac{2\bar{g}_E^2}{1-\mathcal{S}^2}\int d\tau\ \dot{q}_1\dot{q}_2 - \frac{\bar{g}_E^2}{1-\mathcal{S}^2}\int d\tau d\tau' K(\tau-\tau')\sum_{i=1}^{2} q_i(\tau)\sum_{i=1}^{2} q_i(\tau') \quad (19)$$

where $\dot{q}_i = dq_i/d\tau$, M_e denotes the renormalized fluxon mass

$$M_e = M\left(1 - \frac{1}{M}\frac{2\bar{g}_E^2}{1-\mathcal{S}^2}\right) \quad (20)$$

due to the spatially uniform junction-cavity interaction and the M denotes the rest mass of the fluxon. The mass M_e accounts for the renormalization effect of both junction-cavity and magnetic induction interaction. The bare potential $V(q) = V(q_1, q_2)$ is given[33] by

$$V(q) = -\sum_{i=1}^{2}\left(2\pi f_i q_i + \frac{2\epsilon_i}{\cosh^2 q_i}\right) - \frac{8\mathcal{S}(q_1-q_2)}{\sinh(q_1-q_2)}\ . \quad (21)$$

Here, the fluxon potential $V(q)$ includes the effects from the three contributions: (i) the potential tilting effect (f), (ii) the pinning effect (ϵ), and (iii) the magnetic induction effect ($\mathcal{S}$). The third term in [ ] of Eq. (19) accounts for the potential renormalization due to junction-cavity interaction. This renormaliztion is similar to that for the electronic tunneling process with phonon coupling.[34] In the discussion below, we refer $\bar{g}_E^2 = 2\pi^2 g_E^2/M_{osc}$ as the strength of junction-cavity interaction. The cavity kernel $K(\tau-\tau')$ in the third term of Eq. (19) is given by

$$K(\tau) = \frac{\omega_r^3}{2}\ \frac{\cosh(\omega_r/2T - \omega_r|\tau|)}{\sinh(\omega_r/2T)}\ . \quad (22)$$

at non-zero temperature T. This term accounts for the non-local effect arising from the junction-cavity interaction.

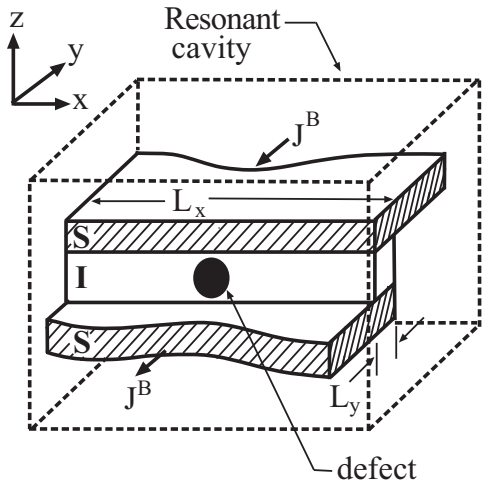

FIG. 1: A LJJ is shown schematically as an insulator (I) layer is sandwiched between two superconductor (S) layers. L_x and L_y denote the dimensions in $x-$ and $y-$direction, respectively. J^B denotes the bias current density. The filled circle represents microresistor (i.e., pinning center), and the dashed box represents resonant cavity.

After the calcultion , the oscillator coordinate q_r in the partition function $\mathcal{Z}$ of Eq. (16) is decoupled from the center coordinate q. This separation allows us to integrate out the q_r-coordinate. Hence, in discussions below, we consider the fluxon contribution $\mathcal{Z}_{fluxon}$ to the partition function which is described by the action S_{eff}. Using S_{eff}, we discuss how the junction-cavity interaction affects both one-fluxon and two-fluxon tunneling in LJJs.

III. MACROSCOPIC QUANTUM TUNNELING IN SINGLE JUNCTION

We now examine the effects of resonant cavity on MQT from the metastable state in a single LJJ obtained by implanting a microresistor in the insulator layer and by applying the bias current (J^B) as shown in Fig. 1. The dimensions of the junction, compared to the Josephson length λ_J, are chosen so that $L_x \gg \lambda_J$ and $L_y \ll \lambda_J$. These choices are made to enhance the quantum effect at low temperatures. We describe MQT of the fluxon by starting with the action $S^s_{eff}[q]$ for the LJJ given by

$$S^s_{eff}[q] = \int d\tau\left[\frac{M_e}{2}\dot{q}^2 + V_s(q) + \bar{g}_E^2\omega_r^2 q^2\right] - \bar{g}_E^2\int d\tau d\tau' K(\tau-\tau')\ q(\tau)q(\tau'). \quad (23)$$

Here, the action $S^s_{eff}[q]$ is obtained from $S_{eff}[q]$ of Eq. (19), by setting $\mathcal{S} = 0$ (i.e., no magnetic induction effect), $q_1 = q$, and $q_2 = 0$. Following Caldeira and Leggett, we may simplify $S^s_{eff}[q]$ by making a usual substitution of

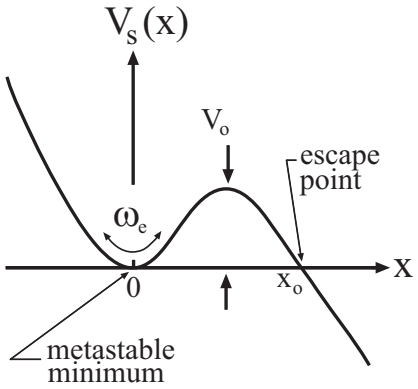

FIG. 2: The fluxon potential V_s due to both the bias current density and microresistor in a single LJJ is schematically illustrated.

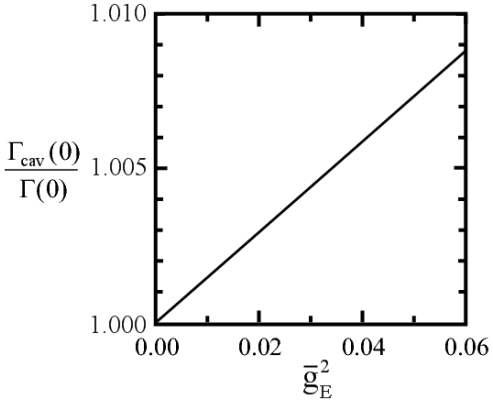

FIG. 3: The ratio of the tunneling rates $\Gamma_{cav}(0)/\Gamma(0)$ is plotted as a function of the junction-cavity coupling strength $\bar{g}_E^2$ to illustrate the size of enhancement.

$q(\tau)q(\tau') = [q^2(\tau) + q^2(\tau')]/2 - [q(\tau) - q(\tau')]^2/2$. We note that the first two terms of this substitution cancel the potential renormalization contribution (i.e., $\bar{g}_E^2\omega_r^2 q^2$ term) arising from the junction-cavity interaction. With this cancellation, the action $S^s_{eff}[q]$ becomes similar to that for the dissipative system,[30] but the fluxon mass is now renormalized to

$$M_e = M\left(1 - \frac{2\bar{g}_E^2}{M}\right) \tag{24}$$

and β is replaced by the junction-cavity interaction strength (i.e., $\beta \to \bar{g}_E^2$). The renormalized mass M_e accounts for the effects of the uniform **E** field in the cavity. The bare fluxon potential $V_s(q)$ is given by

$$V_s(q) = -2\pi f q - \frac{2\epsilon}{\cosh^2 q}. \tag{25}$$

Here the bias current density $f = f_c - \delta_f$ is measured in terms of the deviation δ_f from the critical value $f_c = 4\epsilon/(3\sqrt{3}\pi)$. The potential $V_s(q)$ may be approximated by a quadratic-cubic potential as shown schematically in Fig. 2. The cavity kernel $K(\tau-\tau')$ of Eq. (22) describing the non-local effect due to the junction-cavity interaction simplifies to

$$K(\tau - \tau') = \frac{\omega_r^3}{2} e^{-\omega_r|\tau-\tau'|} \tag{26}$$

in the $T = 0$ limit.

The action $S^s_{eff}[q]$ of Eq. (23) indicates that the resonant cavity yields i) fluxon mass renormalization and ii) non-local effects. The mass renormalization modifies the oscillation frequency about the metastable point, as shown in Fig. 2. This change may be easily seen by computing the oscillation frequency ω_e at the metastatble state (i.e., local minimum) as

$$\omega_e = \left[\frac{1}{M_e}\frac{d^2\bar{V}_s(0)}{dx^2}\right]^{1/2} \approx \omega_o\left(1 + \frac{\bar{g}_E^2}{M}\right), \tag{27}$$

where ω_o is the oscillation frequency at the metastable point in the absence of the resonant cavity. The non-local contribution due to junction-cavity interaction is similar to that for the dissipative system, but to determine the size of this contribution more calculation is needed.

To estimate the size of these two contributions from the junction-cavity interaction, we compute the MQT rate[30,35] given by

$$\Gamma_{cav}(0) = \mathcal{A}_{cav}(0)e^{-\mathcal{B}_{cav}(0)} \tag{28}$$

at $T = 0$. Here, the prefactor $\mathcal{A}_{cav}(0)$ is given by

$$\mathcal{A}_{cav}(0) = \sqrt{60}\,\omega_e\left(\frac{\mathcal{B}_{o,cav}}{2\pi}\right)^{1/2} \tag{29}$$

and the bounce exponent $\mathcal{B}_{cav}(0) = \mathcal{B}_{o,cav} + \delta\mathcal{B}_{cav}$ includes both the local contribution $\mathcal{B}_{o,cav}$ of

$$\mathcal{B}_{o,cav} = \int_{-\infty}^{\infty} d\tau\left[\frac{M_e}{2}\dot{q}^2 + V_s(q)\right] \tag{30}$$

and the non-local contribution $\delta\mathcal{B}_{cav}$ of

$$\delta\mathcal{B}_{cav} = \bar{g}_E^2\int_{-\infty}^{\infty} d\tau\int_{-\infty}^{\infty} d\tau' K(\tau-\tau')\left[q(\tau) - q(\tau')\right]^2 \ . \tag{31}$$

These two contributions, $\mathcal{B}_{o,cav}$ and $\delta\mathcal{B}_{cav}$, to $\mathcal{B}_{cav}(0)$ are evaluated explicitly to estimate their size.

The local contribution $\mathcal{B}_{o,cav}$ may be computed easily by approximating $V_s(q)$ of Eq. (25) as a usual quadratic-plus-cubic potential of

$$\bar{V}_s(x) = V_s(q) - V_s(q_o) \approx \frac{27V_o}{4}\left(\bar{x}^2 - \bar{x}^3\right) \tag{32}$$

where $\bar{x} = x/x_o$, $x = q - q_o$, and $V_o = [8\pi^3\delta_f^3/(\sqrt{3}\epsilon)]^{1/2}$ is the barrier potential for the fluxon. Here q_o is the position of the metastable point and $x_o = 9\sqrt{3}M_e\omega_e^2/32\epsilon$ is the escape point as shown in Fig. 2. The evaluation of $\mathcal{B}_{o,cav}$ yields

$$\mathcal{B}_{o,cav} = 2\int_o^{x_o} dx\left[2M_e\bar{V}_s(x)\right]^{1/2} = \frac{36V_o}{5\omega_e} \ . \tag{33}$$

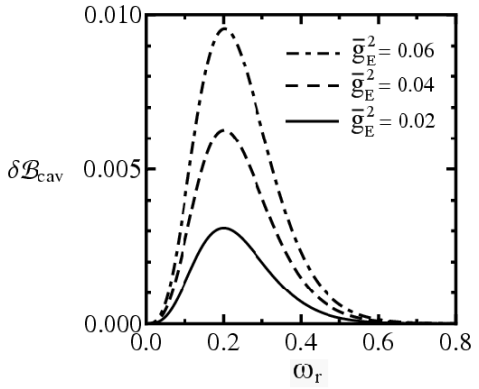

FIG. 4: The non-local contribution $\delta\mathcal{B}_{cav}$ to the bounce exponent $\mathcal{B}_{cav}(0)$ is plotted as a function of ω_r for $\bar{g}_E^2 = 0.02$ (solid line), 0.04 (dashed line) and 0.06 (dot-dashed line).

Using this result, we estimate the local contribution to enhancement of the tunneling rate due to the resonant cavity. The ratio of the MQT rates, $\Gamma_{cav}(0)/\Gamma(0)$, is given by

$$\frac{\Gamma_{cav}(0)}{\Gamma(0)} \approx 1 + \frac{\bar{g}_E^2}{2M}\left(1 + \frac{72}{5}\frac{V_o}{\omega_o}\right) , \qquad (34)$$

where $\Gamma(0)$ is the tunneling rate in the absence of the resonant cavity (i.e., $\bar{g}_E^2 = 0$). Equation (34) indicates that the tunneling rate increases with increasing junction-cavity interaction strength $\bar{g}_E^2$. In Fig. 3, we plot the numerically computed ratio $\Gamma_{cav}(0)/\Gamma(0)$ as a function of $\bar{g}_E^2$ to illustrate its enhancement in the weak-coupling regime (i.e., $\bar{g}_E^2 \ll 1$). The curve indicates that enhancement of $\Gamma_{cav}(0)/\Gamma(0)$ is less than 1%.

The non-local contribution $\delta\mathcal{B}_{cav}$ to $\mathcal{B}_{cav}(0)$ of Eq. (28) reduces the tunneling rate $\Gamma_{cav}(0)$. The size of this reduction is estimated by evaluating $\delta\mathcal{B}_{cav}$ of Eq. (31) by writing

$$\delta\mathcal{B}_{cav} = \frac{\bar{g}_E^2\omega_r^3 x_o^2}{\omega_e^2}\int_{-\infty}^{\infty} d\bar{\tau}d\bar{\tau}' e^{-\frac{2\omega_r}{\omega_e}|\bar{\tau}-\bar{\tau}'|}\left[\bar{x}(\bar{\tau}) - \bar{x}(\bar{\tau}')\right]^2 , \qquad (35)$$

where $\bar{x}(\tau) = \mathrm{sech}^2(\omega_e\tau/2)$. We note that $\bar{x}(\tau)$ is the solution to the equation of motion for the quadratic-plus-cubic potential in the absence of the non-local effect. We evaluate Eq. (35) and obtain

$$\delta\mathcal{B}_{cav} = 2\bar{g}_E^2\left(\frac{9\sqrt{3}M_e}{16\epsilon}\right)^2 \frac{\omega_r^5}{\sinh^2(\pi\omega_r/\omega_e)} . \qquad (36)$$

The result for $\delta\mathcal{B}_{cav}$ indicates that the non-local contribution increases almost linearly with $\bar{g}_E^2$ in the weak-coupling regime and has a strong dependence on the frequency ω_r of the cavity mode. At low cavity frequencies ($\omega_r \ll 1$), the non-local contribution varies as $\delta\mathcal{B}_{cav} \propto \omega_r^3$. At high cavity frequencies ($\omega_r \gg 1$), on the other hand, it varies as $\delta\mathcal{B}_{cav} \propto \omega_r^5 \exp(-2\pi\omega_{\rm r}/\omega_{\rm e})$.

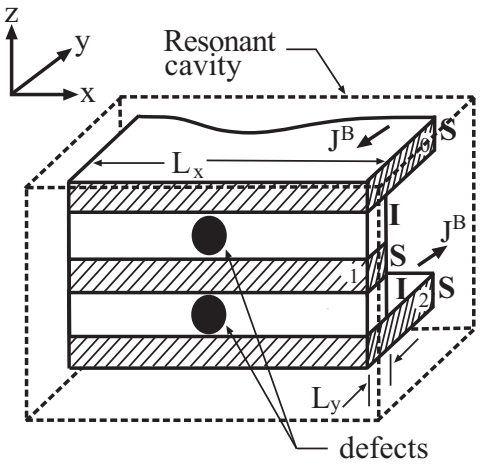

FIG. 5: Two LJJs with a vertical column of two microresistors is shown schematically. L_x and L_y denote the dimensions in $x-$ and $y-$direction, respectively. J^B denotes the bias current density. The filled circles represent the microresistors.

To illustrate the cavity frequency dependence, we plot $\delta\mathcal{B}_{cav}$ as a function of ω_r for $\bar{g}_E^2 = 0.02$ (solid line), 0.04 (dashed line), and 0.06 (dot-dashed line) in Fig. 4. The curves indicate that $\delta\mathcal{B}_{cav}$ vanishes both in the low and high cavity frequency ω_r limits. Hence, the non-local effects on the tunneling rate $\Gamma_{cav}(0)$ is negligible near these limits.

IV. MACROSCOPIC QUANTUM TUNNELING IN COUPLED JUNCTIONS

In this section, we estimate the effects of resonant cavity on the tunneling rate of the phase-locked fluxons from the metastable state in two coupled LJJs. Here the fluxons are trapped by the microresistor on each insulator (I) layer, shown schematically in Fig. 5. Earlier studies[26] indicate that uncorrelated one-fluxon tunneling is the dominant process in the absence of resonant cavity. However, phase-locking between the fluxons in two LJJs becomes enhanced in the resonant cavity. This enhancement may be seen more easily from the effective action $S_{eff}[q]$ for the two coupled LJJs of Eqs. (19) and (21) written in the rotated coordinates (q_+, q_-) as

$$S_{eff}[q] = \int d\tau\left[\frac{M_e}{2}\dot{q}_+^2 + \frac{M}{2}\dot{q}_-^2 + V(\mathbf{q}) + \frac{\bar{g}_E^2\omega_r^2}{1-\mathcal{S}^2}q_+^2\right] - \frac{2\bar{g}_E^2}{1-\mathcal{S}^2}\int d\tau d\tau' K(\tau-\tau')\, q_+(\tau)q_+(\tau'), \qquad (37)$$

where $q_\pm = (q_1 \pm q_2)/\sqrt{2}$. The action $S_{eff}[q]$ indicates that the potential for the in-phase mode, $(q_+, 0)$, is renormalized by the junction-cavity interaction while the out-of-phase mode, $(0, q_-)$, is not. Also, the non-local contribution appears only for the motion in the q_+ direction.

The bare fluxon potential $V(\mathbf{q}) = V(q_+, q_-)$ of

$$V(q_+, q_-) = -2\sqrt{2}\pi f q_+ - \frac{8\sqrt{2}\mathcal{S}q_-}{\sinh\sqrt{2}q_-} - 2\epsilon\left[\frac{1}{\cosh^2\left(\frac{q_+ + q_-}{\sqrt{2}}\right)} + \frac{1}{\cosh^2\left(\frac{q_+ - q_-}{\sqrt{2}}\right)}\right] \quad (38)$$

for $f_1 = f_2 = f$ and $\epsilon_1 = \epsilon_2 = \epsilon$, indicates that the one-dimensional potential along the $(q_+, 0)$ direction (i.e., $V(q_+, 0)$) corresponding to the in-phase mode becomes identical to $V_s(q)$ of Eq. (25) under the transformation of $2f \to f$, $2\epsilon \to \epsilon$, and $q_+/\sqrt{2} \to q$. This similarity reflects that the phase-locked fluxons moving in the $(q_+, 0)$ direction (i.e., $q_1 = q_2$) behave as a single fluxon. However, the one-dimensional potential for the out-of-phase mode (i.e., $V(0, q_-)$ or along the $(0, q_-)$ direction) behaves as a potential well near the metastable point $\mathbf{q}^o = (q_+^o, q_-^o)$, determined from the condition $[\partial V(\mathbf{q})/\partial q_+]_{q_-} = [\partial V(\mathbf{q})/\partial q_-]_{q_+} = 0$.

To illustrate these phase-locking modes, we plot the potential $V(q_+, q_-)$ in Fig. 6 for $f = 0.06$, $\epsilon = 0.269$, and $\mathcal{S} = -0.05$. Here, the value for ϵ and $\mathcal{S}$ are chosen so that when a vertical stack[37] of two interacting JVQs are fabricated using coupled LJJs and microresistors only one quantum state is bound on each side of the double-well potential. The metastable point $\mathbf{q}^o$ is denoted by the solid circle. The solid lines indicate that the potential is metastble for the in-phase mode (i.e., along the $(q_+, 0)$ direction), but it behaves as a well for the out-of-phase mode (i.e., along the $(0, q_-)$ direction). These curves show that tunneling of the in-phase mode from the metastable state is more favorable than that for the out-of-phase mode.

The tunneling rate $\Gamma_{cav}(0)$ from $\mathbf{q}^o$ can be estimated by summing over the contribution from all paths of escape, but the dominant contribution comes from the most probable escape path (MPEP) in which S_{eff} is the minimum.[36] For the physical parameters chosen in Fig. 6, the MPEPs correspond to one-fluxon tunneling, indicated by the dashed lines. The MPEPs are determined by the two competing energies: (i) the pinning energy ($\mathcal{E}_{pin} = |E_{pin}|$) and (ii) the magnetic induction interaction energy ($\mathcal{E}_{int} = |E_{int}|$). When $\mathcal{E}_{int} \gg \mathcal{E}_{pin}$, the fluxons are not pinned at the microresistor sites but maintain a large separation distance.[33] However, when $\mathcal{E}_{int} \ll \mathcal{E}_{pin}$, the one-fluxon tunneling processes are favored over the two-fluxon tunneling processes.

We now estimate the two-fluxon tunneling rate for the in-phase mode. We simplify the calculation by using the simialrity between the tunneling of the in-phase mode and the one-fluxon tunneling process discussed in Sec. III. When the bias current f is less than the critical value f_c (i.e., $f = f_c - \delta_f$ with $0 < \delta_f \ll f_c = 4\epsilon/(3\sqrt{3}\pi)$, the potential along the path $(q_+, 0)$ has the metastable state, as illustrated in Fig. 2. The potential $V(q_+, 0)$ may be

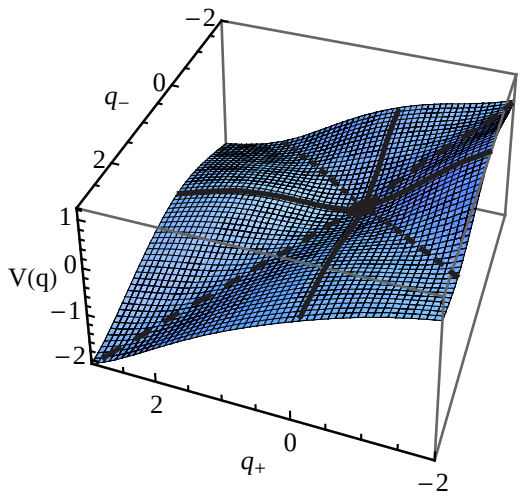

FIG. 6: The potential $V_Q(q_+, q_-)$ surface is plotted for $\epsilon = 0.269$ and $\mathcal{S} = -0.05$. The filled circle represents the position of the metastable state. The dashed and solid lines denote the most probable escape paths (MPEPs) for one-fluxon and two-fluxon tunneling, respectively.

approximated as the quadratic-plus-cubic form of

$$V(\bar{q}_+, 0) \approx \frac{27V_o^t}{4}(\bar{q}_+^2 - \bar{q}_+^3) \ , \quad (39)$$

where $\bar{q}_+ = (q_+ - q_+^o)/q_+^e$, q_+^e is the escape point and $V_o^t = 2[d^2V(q_+^o, 0)/dq_+^2]^3/3[d^3V(q_+^o, 0)/dq_+^3]^2$ denotes the potential barrier height for two-fluxon tunneling. We note that q_+^e is similar to x_o in Fig. 2. Also, similar to the single LJJ, the semiclassically estimated two-fluxon tunneling rate of $\Gamma_{cav}^t(0) = \mathcal{A}_{cav}^t \exp[\mathcal{B}_{cav}^t(0)]$ at $T = 0$ depends on both the barrier height and oscillation frequency. The factor $\mathcal{A}_{cav}^t(0)$ and bounce exponent $\mathcal{B}_{cav}^t(0)$ are calculated in the same way as in Sec. III. The factor $\mathcal{A}_{cav}^t(0)$ is given by

$$\mathcal{A}_{cav}^t(0) \approx \sqrt{60}\ \omega_e \left(\frac{\mathcal{B}_{o,cav}^t}{2\pi}\right)^{1/2} . \quad (40)$$

The local and non-local contributions to the bounce exponents $\mathcal{B}_{cav}^t(0) = \mathcal{B}_{o,cav}^t + \delta\mathcal{B}_{cav}^t$ are given by

$$\mathcal{B}_{o,cav}^t = 2\int_0^{q_+^e - q_+^o} dq_+ \sqrt{2M_e V(q_+, 0)} \approx \frac{36V_o^t}{5\omega_e}, \quad (41)$$

and

$$\delta\mathcal{B}_{cav}^t \approx \frac{2\bar{g}_E^2}{1-\mathcal{S}^2}\left(\frac{9\sqrt{3}M_e}{16\epsilon}\right)^2 \frac{\omega_r^5}{\sinh^2(\pi\omega_r/\omega_e)} \ , \quad (42)$$

respectively. The result indicates that the two-fluxon tunneling rate $\Gamma_{cav}^t(0)$ in the cavity is enhanced from that $\Gamma^t(0)$ in its absence. Neglecting the non-local contribution, we may write the ratio $\Gamma_{cav}^t(0)/\Gamma^t(0)$ as

$$\frac{\Gamma_{cav}^t(0)}{\Gamma^t(0)} \approx 1 + \frac{\bar{g}_E^2}{2M(1-\mathcal{S}^2)}\left(1 + \frac{72}{5}\frac{V_o^t}{\omega_o}\right) . \quad (43)$$

This enhancement is similar to the tunneling process discussed in Sec. III. The estimated value of $\Gamma^t(0)$ for the Nb-Al_2O_x-Nb-Al_2O_x-Nb junction is 8.5×10^9 s^{-1}. This value is obtained by using the experimental value[15,17] of J_c $\sim 2\times 10^6 \mathrm{A/m}^2$, λ_L $\sim$90nm, λ_J $\sim 25\mu$m, and ω_p $\sim$90GHz. Also, we chose $L_y \sim 0.2\mu$m to enhance the quantum effect and used the experimentally accessible value[24] of $\epsilon = 0.269$, $\mathcal{S} = -0.05$ and $\delta_f \sim 5\times 10^{-4}$. On the other hand, the potential $V(q_+, q_-)$ along the $(q_+, 0)$ direction indicates that the two-fluxon tunneling rate $\Gamma^t_{cav}(0)$ is suppressed from the one-fluxon tunneling rate $\Gamma^o_{cav}(0)$ along either the $q_+ = q_-$ or $q_+ = -q_-$ direction. This reduction in the tunneling rate is given by

$$\frac{\Gamma^t_{cav}(0)}{\Gamma^o_{cav}(0)} \approx \alpha_o \sqrt{\frac{V^t_o}{V^o_o}} e^{-\frac{36(V^t_o - \alpha_o^2 V^o_o)}{5\omega_o}} \times \left[1 + \frac{36\bar{g}_E^2 (V^t_o - \alpha_o^2 V^o_o)}{5\omega_o M(1-\mathcal{S}^2)}\right], \quad (44)$$

where $\alpha_o = \{[d^2V(q^o_+,0)/dq^2]/[d^2V(q^o,0)/dq^2]\}^{1/4}$ is a constant of order unity, $V^o_o = 2[d^2V(q^o,0)/dq^2]^3/3[d^3V(q^o,0)/dq^3]^2$ is the one-fluxon tunneling potential barrier height, $V(q,0)$ is the fluxon potential of Eq. (21) along the $q_+ = q_-$ direction, and q^o denotes the position of the metastable point for one-fluxon tunneling, given by the condition that $dV(q^o,0)/dq = 0$. The ratio $\Gamma^t_{cav}(0)/\Gamma^o_{cav}(0) \ll 1$ for the potential surface in Fig. 6 reflects that $V^t_o \gg V^o_o$.

V. JOSEPHSON VORTEX QUBIT IN RESONANT CAVITY

We now examine the effects of high-Q_c resonant cavity on JVQ. The JVQ may be fabricated by using two closely implanted microresistors in the insulator layer of the linear LJJ as shown in Fig. 7. As earlier studies[3–5] indicate, MQT of fluxon between the spatially separated minima of double-well potential leads to splitting of the degenerate ground-state energy.[38,39] In this section, we estimate the effects of junction-cavity interaction on this energy splitting.

The interaction between the LJJ and resonant cavity yields i) fluxon potential renormalization and ii) nonlocal contribution to the action. The effects of these contributions on the energy splitting may be estimated by starting with the action S^Q_{eff} for the JVQ given by

$$S^Q_{eff}[q] = \int d\tau \left[\frac{M_e}{2}\dot{q}^2 + V_Q(q)\right] - 2\bar{g}_E^2 \int d\tau d\tau' \; K(\tau - \tau') \; q(\tau) q(\tau') \; . \quad (45)$$

Without loss of generality, we obtain the potential function $V_Q(q)$ from the double-well potential $V(q)$ of

$$V(q) = \bar{g}_E^2 \omega_r^2 q^2 - \frac{2\epsilon}{\cosh^2\left(q - \frac{\ell}{2}\right)} - \frac{2\epsilon}{\cosh^2\left(q + \frac{\ell}{2}\right)}, \quad (46)$$

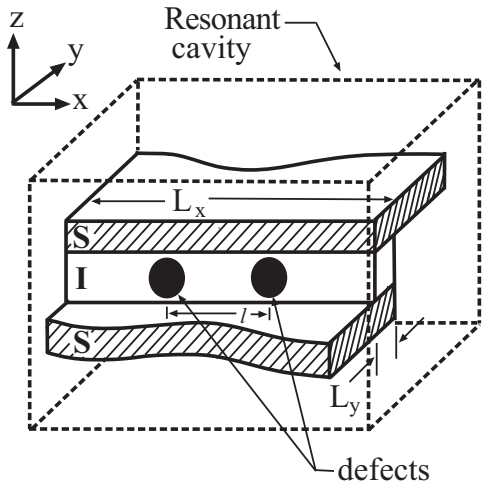

FIG. 7: A LJJ with two microresistors, representing a Josephson vortex qubit, in a resonant cavity is shown schematically. The separation distance between the microresistors is denoted by ℓ. The filled circles and dashed box represent the microresistors and resonant cavity, respectively.

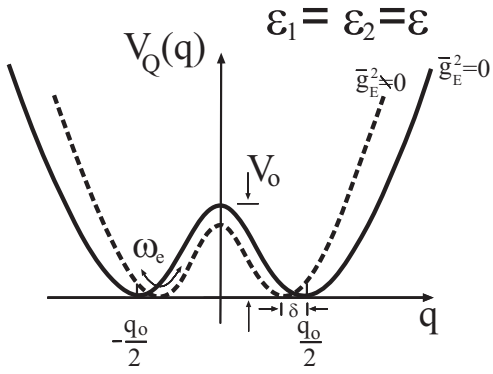

FIG. 8: A schematic diagram of a double-well potential $V_Q(q)$ due to the two microresistors in the insulator layer of the LJJ is shown to illustrate the renormalization of $V_Q(q)$. The solid and dashed lines represent the potential $V_Q(q)$ in the absence and in the presence of the resonant cavity, respectively.

where ℓ denotes the separation distance between the two microresistors. Here, we have added a constant energy E_Q term to $V(q)$ (i.e., $V_Q(q) = V(q) + E_Q$) so that $V_Q(q)$ vanishes at the potenital minima. Here, the potential $V_Q(q)$ may be characterized by the position of the two minima and the potential barrier height. In the discussion below, we do not make the usual substitution of $q(\tau)q(\tau') = [q^2(\tau) + q^2(\tau')]/2 - [q(\tau) - q(\tau')]^2/2$ used in Sec. III. This approach allows us to elucidate the origin of the changes in the energy splitting due to the junction-cavity interaction.

In the absence of the resonant cavity (i.e., $\bar{g}_E^2 = 0$), the double-well structure for $V_Q(q)$ with the separation distance $\ell > \ell_o \approx 1.317$ is shown schematically in Fig. 8

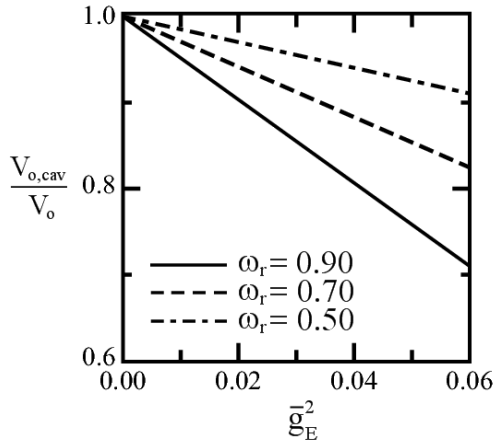

FIG. 9: The ratio of the potential barrier height $V_{o,cav}/V_o$ is plotted as a function of the junction-cavity coupling strength $\bar{g}_E^2$ for $\omega_r = 0.50$ (dot-dashed line), 0.70 (dashed line), and 0.90 (solid line) to illustrate the suppression in the cavity.

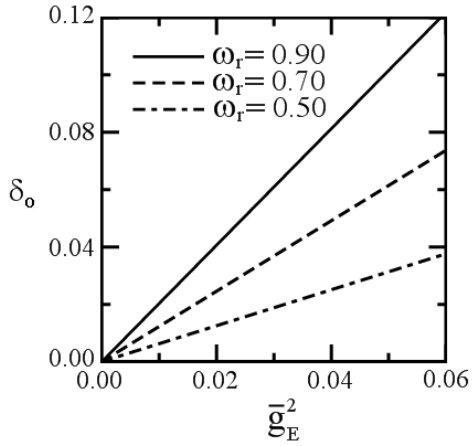

FIG. 10: The shift δ_o in the position of the potential minima is plotted as a function of the junction-cavity coupling strength $\bar{g}_E^2$ for $\omega_r = 0.50$ (dot-dashed line), 0.70 (dashed line), and 0.90 (solid line).

as the solid line. The two potential minima are located at $q = \pm q_o/2$ where q_o is determined from

$$\cosh q_o = \frac{\sinh^2 \ell - 1}{\cosh \ell} \ . \tag{47}$$

The energy shift E_Q, representing a constant of motion, is given by

$$E_Q = -2\epsilon \frac{\cosh^2 \ell}{\cosh^2 \ell - 1} \ . \tag{48}$$

Also, the potential barrier height V_o between the two minima (i.e., $q = \pm q_o/2$) is given by

$$V_o = 2\epsilon \left(\frac{\cosh \ell - 2}{\sinh \ell} \right)^2 \ . \tag{49}$$

We note that these quantities change in the resonant cavity, as shown schematically by the dashed line in Fig. 8.

In the resonant cavity (i.e., $\bar{g}_E^2 \neq 0$), on the other hand, the JVQ potential $V_Q(q)$ acquires an additional $\bar{g}_E^2 \omega_r^2 q^2$ term in Eq. (46). This term arises from the coupling between the oscillator coordinate q_r and the center coordinate q in the coupling Lagrangian $\mathcal{L}_{coup}$ of Eq. (15) and accounts for potential renormalization. The main renormalization effects are the following: i) the barrier potential height is reduced, ii) the position of the potential minima become closer together, and iii) the oscillation frequency at the potential minima is modified. These effects become amplified with increasing junction-cavity interaction strength ($\bar{g}_E^2$) and resonant frequency (ω_r).

The effects of the junction-cavity interaction on the potential barrier height $V_{o,cav}$ may be estimated straightforwardly. In Fig. 9, we plot the numerically computed ratio $V_{o,cav}/V_o$ as a function of $\bar{g}_E^2$ to illustrate the dependence on the junction-cavity interaction. The curves for $\omega_r = 0.50$ (dot-dashed line), 0.70 (dashed line) and 0.90 (solid line) indicate that the barrier potential height decreases with increasing $\bar{g}_E^2$ and ω_r. Also, the curves indicate that the ratio decreases linearly in the weak coupling regime. To leading order in $\bar{g}_E^2$, the potential barrier height $V_{o,cav}$ estimated from the renormalized potential $V(q)$ of Eq. (46) is given by

$$V_{o,cav} \cong V_o - \bar{g}_E^2 \omega_r^2 q_o^2 \ . \tag{50}$$

This decrease in the potential barrier height leads to the increase in the ground-state energy splitting.

Another important effect of the resonant cavity is the shift δ_o in the position of potential minima. As the potential barrier height is reduced, the position of the potential minima are closer together. The shift δ_o from the initial position of $q = \pm q_o/2$ is given by

$$\delta_o = \frac{\bar{g}_E^2 q_o \omega_r^2}{\epsilon} \frac{\cosh^2 \ell \tanh^2 \ell}{\cosh 2\ell - 7} \ . \tag{51}$$

Here, we obtained δ_o by imposing the condition $[dV(q)/dq|_{q=(q_o/2)_\pm} = 0$, where $(q_o/2)_\pm = \pm[(q_o/2) - \delta_o]$ denotes the new potential minima. This shift δ_o modifies the constant of motion E_Q. The new value for E_Q may be obtained from the condition $[dq(\tau)/d\tau]_{(q_o/2)_\pm} = 0$, noting that the fluxon is initially located at the bottom of either side of the double-well potential so that $V_Q((q_o/2)_\pm) = 0$. We plot the numerically computed shift δ_o as a function of $\bar{g}_E^2$ in Fig. 10 for $\omega_r = 0.50$ (dot-dashed line), 0.70 (dashed line), and 0.90 (solid line) to illustrate the amount of this shift in the weak-coupling regime. The curves indicate that δ_o increases with $\bar{g}_E^2$ and with ω_r, reflecting potential renormalization.

The resonent cavity also modifies the oscillation frequency ω_e at the potential minima. The modified frequency ω_e is given by

$$\omega_e \approx \omega_o \left\{ 1 + \frac{\bar{g}_E^2}{M} \left[1 + \frac{\omega_r^2}{\omega_o^2} (1 - \Upsilon) \right] \right\} \ , \tag{52}$$

where ω_o is the frequency in the absence of resonant cavity and $\Upsilon = 6q_o \sinh 2q_o \tanh \ell/\epsilon(\cosh^2 \ell - 4)\sinh^2 \ell$.

We now combine these effects together and estimate the ground-state energy splitting[38] Δ_{cav} by using the action $S^Q_{eff}[q]$ of Eq. (45) and by using the standard method of summing over the "instanton" trajectories.[40] By following Weiss and coworkers,[41] we compute the one-bounce contribution to the partition function $\mathcal{Z}_{fluxon}$, assuming that the fluxon is initially pinned at one of the potential minima. We write the partition function as

$$\mathcal{Z}_{fluxon} = \sum_{i=0}^{\infty} \mathcal{Z}_i \tag{53}$$

where $\mathcal{Z}_i$ denotes the i-bounce contribution. Here the bounce is an instanton-anti-instanton pair. To estimate Δ_{cav}, we compute both the saddle-point ($\mathcal{Z}_0$) and the one-bounce ($\mathcal{Z}_1$) contribution to $\mathcal{Z}_{fluxon}$ by noting that $\mathcal{Z}_1$ may be expressed as

$$\mathcal{Z}_1 = \frac{\mathcal{Z}_0}{2\pi}\left(\frac{\Delta_{cav}\theta}{2}\right)^2 , \tag{54}$$

where $\theta = 1/T$. For the contribution $\mathcal{Z}_0$, we assume that the fluxon is initially confined at $q = (q_o/2)_-$ and obtain

$$\mathcal{Z}_0 = N\left(\prod_{n=0}^{\infty}\lambda_n^o\right)^{-1/2} \tag{55}$$

where the eigenvalues λ_n^o are determined from

$$\left[-M_e\partial_\tau^2 + V_Q^{''}\left(-\frac{q_o}{2}+\delta\right)\right] q_n^o(\tau) + 4\pi\bar{g}_E^2\int_{-\theta/2}^{\theta/2} K(\tau-\tau')\; q_n^o(\tau') = \lambda_n^o q_n^o(\tau). \tag{56}$$

Here $\partial_\tau^2 = \partial^2/\partial\tau^2$, $V_Q^{''}(q) = \partial^2 V_Q(q)/\partial q^2$, and the cavity kernel $K(\tau-\tau') = (\omega_r^3/2)\exp[-\omega_r|\tau-\tau'|]$ accounts for the non-local effect.

For the one-bounce contribution $\mathcal{Z}_1$ to $\mathcal{Z}_{fluxon}$, we separate the center coordinate $q(\tau)$ into two parts as

$$q(\tau) = \bar{q}(\tau) + \sum_{n=0}^{\infty} c_n q_n(\tau) , \tag{57}$$

where $\bar{q}(\tau)$ describes a bounce-like trajectory and the remaining terms describe the arbitrary paths about this bounce-like trajectory. This separation of $q(\tau)$ may be used to write the action $S^Q_{eff}[q]$ as

$$S^Q_{eff}[q(\tau)] = S^{cav}_{B,1}(\bar{q}(\tau)) + \sum_{n=0}^{\infty}\frac{1}{2}\lambda_n c_n^2 . \tag{58}$$

Here $S^{cav}_{B,1}$ accounts for the one-bounce-like trajectory in the resonant cavity. We choose $q_n(\tau)$ of Eq. (57) so that the eigenfunctions of the second variational derivative of $S^Q_{eff}[q]$ at $\bar{q}$ and the eigenvalues λ_n are determined from

$$\left[-M_e\partial_\tau^2 + V_Q^{''}(\bar{q})\right] q_n(\tau) + 4\pi\bar{g}_E^2\int_{-\theta/2}^{\theta/2} K(\tau-\tau')\; q_n(\tau') = \lambda_n q_n(\tau). \tag{59}$$

We note that the first two eigenvalues, λ_0 and λ_1, need to be separated from the rest because $\lambda_0 \le 0$ and $\lambda_1 = 0$ while the other eigenvalues are positive. The one-bounce contribution ($\mathcal{Z}_1$) may be expressed as

$$\mathcal{Z}_1 = N\int\prod_{n=0}^{\infty}\frac{dc_n}{\sqrt{2\pi}} e^{-\left(S^{cav}_{B,1} + \frac{1}{2}\sum_{n=0}^{\infty}\lambda_n c_n^2\right)} , \tag{60}$$

where N is a normalization constant. With the separation of the first two eigenvalues (i.e., $\lambda_0 \le 0$ and $\lambda_1 = 0$) from the others, we write the one-bounce contribution to the partition function as

$$\mathcal{Z}_1 \approx \frac{\mathcal{Z}_0\theta}{2\pi}\left[\int_0^{\theta} d\tau_1 e^{-S^{cav}_{B,1}(\tau_1)}\right]\left[\frac{\prod_{n=0}^{\infty}\lambda_n^o}{\prod_{n=2}^{\infty}\lambda_n}\right]^{1/2}\times \left[\int_{-\theta/2}^{\theta/2} d\tau\left(\frac{d\bar{q}}{d\tau_1}\right)^2\right]^{1/2}\left[\int_{-\theta/2}^{\theta/2} d\tau'\left(\frac{d\bar{q}}{d\tau'}\right)^2\right]^{1/2} . \tag{61}$$

We now need to evaluate $\mathcal{Z}_1$ of Eq. (61) to estimate Δ_{cav}. Using Eq. (54), we write the ground-state energy splitting Δ_{cav} as

$$\Delta_{cav} = \frac{2\omega_e}{\sqrt{\pi}}\left(R_{cav}L_{cav}e^{-S^{cav}_{B,1}}\right)^{1/2} \tag{62}$$

where the dimensionless factors R_{cav} and L_{cav} are

$$R_{cav} = \frac{1}{M_e\omega_e^2}\left(\frac{\prod_{n=0}^{\infty}\lambda_n^o}{\prod_{n=2}^{\infty}\lambda_n}\right)^{1/2} \tag{63}$$

and

$$L_{cav} = \frac{M_e}{2}\left[\int d\tau\left(\frac{d\bar{q}}{d\tau_1}\right)^2\right]^{1/2}\left[\int d\tau'\left(\frac{d\bar{q}}{d\tau'}\right)^2\right]^{1/2} , \tag{64}$$

respectively. The exponent $S^{cav}_{B,1}$ is given by

$$S^{cav}_{B,1} = \int_{-\theta/2}^{\theta/2} d\tau\left[\frac{M_e}{2}\left(\frac{dq(\tau)}{d\tau}\right)^2 + V_Q(q)\right] . \tag{65}$$

This exponent accounts for the contribution from the two transversal of the potential barrier. We note that the exponent $S^{cav}_{B,1}$ of Eq. (65) does not contain the non-local contribution, as in Eq. (28), because this contribution is already included in the calculation of $\mathcal{Z}_1$ (see Eq. (60)). We now compute R_{cav}, L_{cav} and $S^{cav}_{B,1}$, separately, to determine the ground-state energy splitting Δ_{cav}. To focus on the effects due to the junction-cavity interaction, we

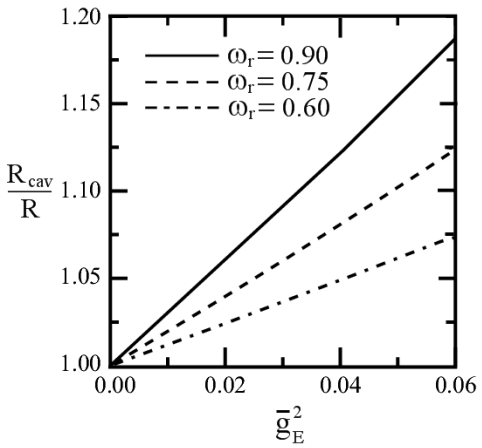

FIG. 11: The numerically computed ratio of the dimensionless factor R_{cav}/R is plotted as a function of the junction-cavity coupling strength $\bar{g}_E^2$ for $\omega_r = 0.60$ (dot-dashed line), 0.75 (dashed line), and 0.90 (solid line).

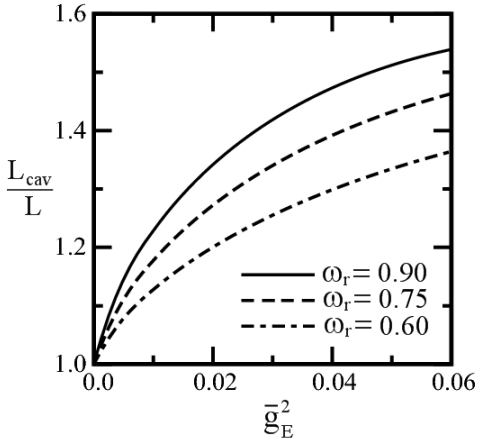

FIG. 12: The numerically computed ratio of L_{cav}/L is plotted as a function of the junction-cavity coupling strength $\bar{g}_E^2$ for $\omega_r = 0.60$ (dot-dashed line), 0.75 (dashed line), and 0.90 (solid line) to illustrate the enhancement.

present the details of the calculation for R_{cav} and L_{cav} in Appendix A and B, respectively, and discuss the dependence of these factors on the junction-cavity coupling strength $\bar{g}_E^2$.

The dimensionless factor R_{cav} in the weak-coupling regime is given by

$$R_{cav} \cong 2 + \frac{\pi \bar{g}_E^2 \omega_r^2}{2M\omega_o^2} \frac{X_R}{(\omega_r + \omega_o)^3} \ , \tag{66}$$

where $X_R = \omega_r^3 + 15\omega_r^2\omega_o + 12\omega_r\omega_o^2 - 2\omega_o^3$. Equation (66) yields the value $R_{cav} = 2$ in the absence of resonant cavity (i.e., $\bar{g}_E^2 = 0$).[39] In Fig. 11, we plot the numerically computed ratio R_{cav}/R as a function of $\bar{g}_E^2$ for $\omega_r = 0.60$ (dot-dashed line), 0.75 (dashed line), and 0.90 (solid line) to illustrate enhancement of R due to resonant cavity. The curves indicate that R_{cav}/R increases from 1 almost linearly with increasing $\bar{g}_E^2$ and ω_r.

For the dimensionless factor L_{cav}, we evaluate the integral of Eq. (64) by expanding the function $Q(\tau)$ which accounts for the non-local contribution to the bounce-like trajectory as a power series. (See Appendix B.) In the weak-coupling regime (i.e., $\bar{g}_E^2 \ll 1$), we obtain

$$L_{cav} \approx \mathcal{V}_M[A_o + \bar{g}_E^2(B_0 + B_2 q_o^2 + B_4 q_o^4)] \ , \tag{67}$$

by retaining the leading order contribution (in $\bar{g}_E^2$). Here $\mathcal{V}_M = q_o\sqrt{2MV_o}$, $A_o = 1 - q_o^2(2\epsilon b_1/3V_o) - q_o^4(4\epsilon b_2/15V_o)$, $B_0 = -(\epsilon + 8b_3\omega_r^2)/8\epsilon$, $B_2 = [b_1\epsilon + 2(6b_1b_3 - 1)\omega_r^2 + 2\pi d_1\omega_r^3]/6V_o$, and $B_4 = [b_2\epsilon + 20b_2b_3\omega_r^2 + \epsilon) + 3\pi d_3\omega_r^3]/15V_o$. The frequency independent constants b_i are $b_1 = (\cosh\ell - 2)\mathrm{sech}^4(\ell/2)$, $b_2 = (\cosh 2\ell - 26\cosh\ell + 33)/(\cosh\ell + 1)^3$, and $b_3 = (\sinh\ell\tanh\ell)^2/(\cosh 2\ell - 7)$. Equation (67) indicates that L_{cav} in the resonant cavity is larger than $L = \mathcal{V}_M A_o$ in its absence. However, due to the functional form of L_{cav}, the enhancement of L_{cav} from L deviates from the linear dependence on $\bar{g}_E^2$ at a smaller value than that for R_{cav}. To illustrate this deviation, we numerically compute L_{cav} and plot the ratio L_{cav}/L in Fig. 12 as a function of $\bar{g}_E^2$ for $\omega_r = 0.60$ (dot-dashed line), 0.75 (dashed line), and 0.90 (solid line). The curves show nonlinear enhancement of the dimensionless factor L_{cav} for much smaller value of $\bar{g}_E^2$ than that for R_{cav} shown in Fig. 11.

Finally, we estimate the effects of junction-cavity interaction on $S_{B,1}^{cav}$. The action $S_{B,1}^{cav}$ of Eq. (65) for the bounce-like trajectory is given by

$$S_{B,1}^{cav} = 2\int_{(q_o/2)_-}^{(q_o/2)_+} dq\sqrt{2M_e V_Q(q)} \ . \tag{68}$$

The integral of Eq. (68) is evaluated in the same way as that for L_{cav} (see Appendix B). Again, we simplify the calculation by writing V_Q as a power series in q and then expand $\sqrt{V_Q(q)}$ in powers of $\bar{g}_E^2$ as

$$\sqrt{V_Q} \approx \frac{\mathcal{V}_M}{\sqrt{2M_e}q_o}\Bigg\{1 - \frac{2\epsilon q^2}{V_o}\left(b_1 + \frac{4b_2}{3}q^2 + \cdots\right) - \bar{g}_E^2\left[\frac{1}{8} + \frac{\omega_r^2 q_o^2}{2V_o} - \frac{\epsilon q^2}{2V_o}\left(\bar{b}_1 + \frac{2}{3}b_2 q^2\right)\right]\Bigg\}, \tag{69}$$

where $\bar{b}_1 = b_1 + (\omega_r^2/\epsilon)$. Using this series expansion for $\sqrt{V_Q}$, we evaluate Eq. (68) and obtain $S_{B,1}^{cav}$ to the leading order in $\bar{g}_E^2$ as

$$S_{B,1}^{cav} \approx 4\mathcal{V}_M[A_o + \bar{g}_E^2(B_0 + \bar{B}_2 q_o^2 + \bar{B}_4 q_o^4)] \ , \tag{70}$$

where $\bar{B}_2 = B_2 - (\pi d_1\omega_r^3/3V_o)$ and $\bar{B}_4 = B_4 - (3\pi d_3\omega_r^3/15V_o)$. The action $S_{B,1}^{cav}$ in the presence of cavity is reduced from that in its absence (i.e., $S_{B,1}^{cav} < S_{B,1}$). To illustrate this suppression of the ratio, we plot the numerically computed ratio $S_{B,1}^{cav}/S_{B,1}$ as a function of $\bar{g}_E^2$ for $\omega_r = 0.60$ (dot-dashed line), 0.75 (dashed line), and 0.90 (solid line) in Fig. 13. The curves indicate that

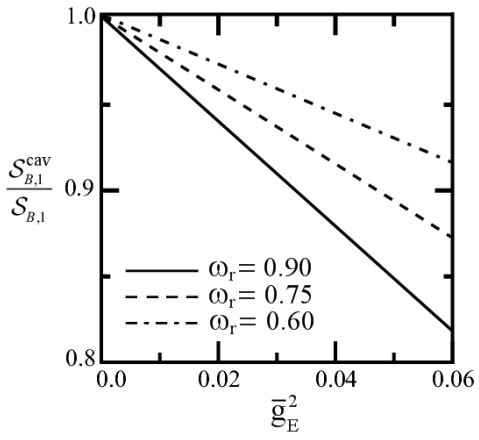

FIG. 13: The numerically computed ratio of the action $S^{cav}_{B,1}/S_{B,1}$ is plotted as a function of $\bar{g}^2_E$ for $\omega_r = 0.60$ (dot-dashed line), 0.75 (dashed line), and 0.90 (solid line) to illustrate that the one-bounce-like action is reduced.

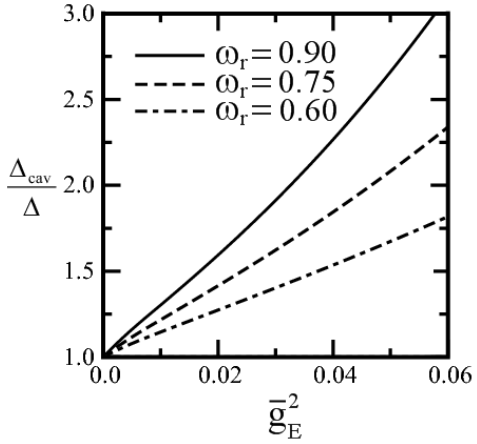

FIG. 14: The numerically computed ratio of Δ_{cav}/Δ is plotted as a function of the junction-cavity coupling strength $\bar{g}^2_E$ for $\omega_r = 0.60$ (dot-dashed line), 0.75 (dashed line) and 0.90 (solid line) to illustrate the enhancement in resonant cavity.

in the one-bounce contribution to the action decreases almost linearly with $\bar{g}^2_E$ in the weak-coupling region as indicated by Eq. (70). This reduction reflects that the potential barrier height is reduced (see Fig. 9) and the potential minima become closer together (see Fig. 10) with increasing junction-cavity interaction strength.

We now combine the effects of resonant cavity on R_{cav}, L_{cav} and $S_{B,1}$ together and estimate the enhancement of the gound-state energy splitting Δ_{cav} from Δ. Here, Δ denotes the energy splitting in the absence of resonant cavity given by

$$\Delta = 2\mathcal{A}\left(\frac{S_o}{2\pi}\right)^{1/2} e^{-S_o}, \tag{71}$$

where $\mathcal{A} = [\prod_{n=0}^{\infty}\lambda_n^o/\prod_{n=1}^{\infty}\lambda_n]^{1/2}$ and S_o denotes the action integral. In the weak-coupling regime, the ratio Δ_{cav}/Δ to the leading order in $\bar{g}^2_E$ is given by

$$\frac{\Delta_{cav}}{\Delta} \approx 1 + \frac{\bar{g}^2_E}{M}\Bigg\{1 \;+\; \frac{\omega_r^2}{\omega_o^2}\left[1 - \Upsilon + \frac{\pi X_R}{8(\omega_r+\omega_o)^3}\right] + \frac{M}{2A_o}(B_0 + B_2 q_o^2 + B_4 q_o^4) - 2M\mathcal{V}_M(B_0 + \bar{B}_2 q_o^2 + \bar{B}_4 q_o^4)\Bigg\}. \tag{72}$$

The result indicates that Δ_{cav} is enhanced with increasing $\bar{g}^2_E$ and ω_r. To illustrate this enhancement, we numerically compute and plot Δ_{cav}/Δ as a function of $\bar{g}^2_E$ for $\omega_r = 0.60$ (dot-dashed line), 0.75 (dashed line) and 0.90 (solid line) in Fig. 14. The curves show that Δ_{cav}/Δ increases roughly linearly with $\bar{g}^2_E$ from $\bar{g}^2_E = 0$ to 0.02. However, the deviation from this linear behavior becomes noticeable for $\bar{g}^2_E \geq 0.02$. Also, Δ_{cav}/Δ increases significantly from 1 at $\bar{g}^2_E = 0$ in the weak-coupling regime. We note that the corresponding changes in the ratio R_{cav}/R, L_{cav}/L and $S^{cav}_{B,1}/S_{B,1}$ over the same range of $\bar{g}^2_E$ are less significant. For instance, Δ_{cav}/Δ for $\omega_r = 0.90$ increases from 1.0 to 1.45 for the increase of $\bar{g}^2_E$ from 0.0 to 0.015. Over the same range of $\bar{g}^2_E$, R_{cav}/R, L_{cav}/L and $S^{cav}_{B,1}/S_{B,1}$ change from 1.0 to 1.05, from 1.0 to 1.29, and from 1.0 to 0.96, respectively. The notable increase in Δ_{cav}/Δ compared to R_{cav}/R, L_{cav}/L and $S^{cav}_{B,1}/S_{B,1}$ reflects that Δ is small.[4] Hence, Δ_{cav} depends sensitively on the variation of the exponent $S^{cav}_{B,1}$.

VI. SUMMARY AND CONCLUSION

In summary, we investigated the effects of high-Q_c resonant cavity on MQT of fluxon from metastable state in a single LJJ and in a stack of two coupled LJJs. Also, we estimated the ground-state energy splitting for fluxon in a double-well potential. We find that both the tunneling rate and the ground-state energy splitting are increased in the resonant cavity. However, the amount of these increases is significantly different. For MQT of the fluxon, the tunneling rate increases due to the renormalization of fluxon mass, but negligible in the weak-coupling regime. On the other hand, the increase in the ground-state energy splitting is due to potential renormalization, but this increase can become significant with increasing $\bar{g}^2_E$ as shown in Fig. 14. This energy splitting enhancement is consistent with the result of increase in the energy separation due to the interaction between a two-level system and a quantized radiation field, described by the Jaynes-Cummings (JC) model.[28] Moreover, the consistency[42] between the result of the present work and that of the JC model indicates that the effective Hamiltonian for the JVQ-cavity system may be similar to the JC model.

The effects due to i) interaction between the JVQ and a dissipative environment and ii) the losses resulting from a low-Q cavity are neglected in the present work. These dissipative effects are expected to be present in real sys-

tems and may be accounted by using an effective spectral density which characterizes the form of dissipation.[43] Inclusion of both the dissipative environment and cavity losses may reduce the size of increase in the ground-state energy splitting and may lead to decrease in the energy spliting when the dissipative effects become strong, as indicated by the analysis of dissipative two-state systems.[31] However, these dissipation contributions do not reverse the effects due to the potential renormalization completely in weakly dissipative systems.

Enhancement of ground-state energy splitting due to the junction-cavity interaction may have an important consequence for the decoherence time of JVQ in the resonant cavity. Earlier study[4] of the JVQ decoherence time by Kim, Dhungana and Park indicates that the increase in the decoherence time in noisy environment (i.e., T_ϕ^{noise}) is correlated with the increasing ground-state energy splitting Δ. This suggests that, as Δ may be tuned by adjusting the strength of junction-cavity interaction, the resonant cavity may be used to control the property of JVQ. For instance, the decoherence time T_ϕ^{noise} may be increased by increasing the strength of interaction between fluxon and cavity EM mode. Also, due to the similarities between a cavity EM mode and an optical phonon mode, the interaction between fluxon and optical phonons in the LJJ may affect the decoherence time.

Another important property of JVQs is entanglement between the qubits. As our result suggests that the decoherence time for JVQ can be increased by increasing the strength of junction-cavity interaction, the resonant cavity may also be useful for tuning the level of entanglement between the JVQs. Our study suggests that the present approach for JVQs is similar to the microwave cavity approach used for the other superconductor qubits.[44] The effective Hamiltonian for the multiple JVQs in a resonant cavity may resemble the Tavis-Cummings model[45] which is the extension of the JC model to the case of multiple qubits. This similarity may be exploited by using the resonant cavity to control the level of concurrence[46] for JVQs since the junction-cavity interaction may also promote entanglement. Hence, the effects of resonant cavity on entanglement between the interacting JVQs would be an interesting area for further study.

The authors would like to thank W. Schwalm and K.-S. Park for helpful discussions and I. D. O'Bryant for assisting with part of the numerical calculation.

APPENDIX A: CALCULATION OF R_{cav}

For convenience, the dimensionless factor R_{cav} of Eq. (63) is estimated in the continuum limit. In this limit, we may write R_{cav} as

$$R_{cav} = \exp\left\{\frac{1}{\pi}\int_{M_e\omega_e^2}^{\infty}\frac{d\lambda}{\lambda}[\delta_+(\lambda)+\delta_-(\lambda)]\right\}, \qquad (73)$$

where $\delta_\pm(\lambda)$ denotes the phase shift due to the scattering potential U. This phase shift may be expressed as

$$\delta_\pm(\lambda) = \cot^{-1}\left[\frac{U^{-1} - g'_\lambda(0) \mp g'_\lambda(\tau_s)}{g''_\lambda(0) \pm g''_\lambda(\tau_s)}\right], \qquad (74)$$

where $\tau_s = -\theta/2$, and $g'_\lambda(\tau)$ and $g''_\lambda(\tau)$ denote the real and imaginary part of the Green's function (i.e., $g_\lambda(\tau) = g'_\lambda(\tau) + ig''_\lambda(\tau)$). The phase shift $\delta_\pm(\lambda)$ due to the scattering from the net potential difference of

$$V''_Q(\bar{q}) - V''_Q((q_o/2)_-) = - U\left[\delta\left(\tau+\frac{\tau_s}{2}\right)+\delta\left(\tau-\frac{\tau_s}{2}\right)\right] \qquad (75)$$

consists of two Dirac δ-functions at $\tau = \pm\tau_s/2$. The strength of the scattering potential U is given by

$$U^{-1} = g_0(0) - g_0(\tau_s), \qquad (76)$$

where $g_0(\tau)$ is the Green's function for the eigenvalue $\lambda = 0$. The Green's function $g_\lambda(\tau)$ is written as

$$g_\lambda(\tau) = \int_{-\infty}^{\infty}\frac{d\omega}{2\pi}\frac{e^{i\omega\tau}}{M_e[\omega^2+\zeta(\omega)+\omega_e^2]-\lambda-i\delta}. \qquad (77)$$

Here the effects of the resonant cavity are accounted for via M_e, ω_e and $\zeta(\omega)$. The function $\zeta(\omega)$, obtained from the cavity kernel $K(\tau)$ of Eq. (26),

$$\zeta(\omega) = \frac{4\pi\bar{g}_E^2}{M_e}\frac{\omega_r^4}{\omega^2+\omega_r^2}, \qquad (78)$$

reflects that the resonant cavity supports a single-mode with frequency ω_r. Using the function $\zeta(\omega)$, we write the real part of the Green's function as $g'_\lambda(\tau) = g'_{\lambda,+}(\tau) + g'_{\lambda,-}(\tau)$, where

$$g'_{\lambda,\pm}(\tau) = \frac{-1}{4M_e\omega_{\lambda,\pm}}\left(1\pm\frac{\omega_r^2+\omega_{1,\lambda}^2}{2\omega_{2,\lambda}^2}\right)\sin\omega_{\lambda,\pm}\tau, \qquad (79)$$

$\omega_{\lambda,\pm} = (\omega_{1,\lambda}^2 \pm \omega_{2,\lambda}^2)^{1/2}$, $\omega_{1,\lambda}^2 = [(\lambda/M_e) - \omega_e^2 - \omega_r^2]/2$, and $\omega_{2,\lambda}^2 = \{[(\lambda/M_e) - \omega_e^2 + \omega_r^2]^2 - (16\pi g_E^2/M_e)\omega_r^4\}^{1/2}$. On the other hand, we write the imaginary part of the Green's function as $g''_\lambda(\tau) = g''_{\lambda,+}(\tau) + g''_{\lambda,-}(\tau)$, where

$$g''_{\lambda,\pm}(\tau) = \frac{1}{4M_e\omega_{\lambda,\pm}}\left(1\pm\frac{\Omega^2+\omega_{1,\lambda}^2}{2\omega_{2,\lambda}^2}\right)\cos\omega_{\lambda,\pm}\tau. \qquad (80)$$

We note that the phase shift $\delta_\pm(\lambda)$ has both slowly varying and rapidly oscillating contributions. For an extended bounce (i.e., $\omega_e\tau_s \gg 1$), the rapidly oscillating terms become negligible compared to the non-oscillating terms.

The factor R_{cav} of Eq. (73) may be simplified by using the substitution $\lambda = M_e\omega_e^2(1+p^2)$, where p is a dimensionless momentum variable. With this change of variable, we write R_{cav} as

$$R_{cav} = \exp\left\{\frac{1}{\pi}\int_0^{\infty}\frac{p\,dp}{1+p^2}[\delta_+(p)+\delta_-(p)]\right\}. \qquad (81)$$

The factor R_{cav} of Eq. (81) may be further simplified by neglecting the rapidly oscillating contributions in the phase shift $\delta_{\pm}(\lambda)$ of Eq. (74). Neglecting these oscillatory contributions, we approximate $\delta_{\pm}(p)$ to a simpler form $\delta(p)$ and write the factor R_{cav} as

$$R_{cav} = \exp\left\{\frac{2}{\pi}\int_0^\infty \frac{p\ dp}{1+p^2}\delta(p)\right\} . \quad (82)$$

The simplified phase shift $\delta(p)$ is given by

$$\delta(p) = \cot^{-1}\left[\frac{U^{-1} - g'_p(0)}{g''_p(0)}\right] , \quad (83)$$

where the scattering potential strength U is given by

$$U^{-1} = \frac{1}{4M_e}\left(\frac{1-W_0}{\sqrt{\omega_{2,0}^2-\omega_{1,0}^2}} + \frac{1+W_0}{\sqrt{|\omega_{2,0}^2+\omega_{1,0}^2|}}\right) , \quad (84)$$

and $W_0 = (\omega_r^2+\omega_{1,0}^2)/\omega_{2,0}^2$. We note that $\omega_{1,0}$ and $\omega_{2,0}$ are obtained from $\omega_{1,\lambda}$ and $\omega_{2,\lambda}$ of Eq. (79) for the eigenvalue $\lambda = 0$, respectively. The real and imaginary part of the Green's function are given, respectively, by

$$g'_p(0) = \frac{1}{4M_e}\frac{1-W_p}{\sqrt{\omega_{2,p}^2-\omega_{1,p}^2}} \quad (85)$$

and

$$g''_p(0) = \frac{1}{4M_e}\frac{1+W_p}{\sqrt{\omega_{2,p}^2+\omega_{1,p}^2}} , \quad (86)$$

where $W_p = (\omega_r^2+\omega_{1,p}^2)/\omega_{2,p}^2$. We note that $\omega_{1,p}$ and $\omega_{2,p}$ are obtained from $\omega_{1,\lambda}$ and $\omega_{2,\lambda}$ of Eq. (79), respectively, by setting $\lambda = M_e\omega_e^2(1+p^2)$.

We now compute R_{cav} to the leading order in $\bar{g}_E^2$ to account for the effects of resonant cavity in the weak coupling regime (i.e., $\bar{g}_E^2 \ll 1$). For this calculation, we write the renormalized mass of the fluxon as $M_e = M - 2\bar{g}_E^2$ and express the oscillation frequency ω_e as

$$\omega_e^2 \cong \omega_o^2\left\{1 + \frac{2\bar{g}_E^2}{M}\left[1 + \frac{\omega_r^2}{\omega_o^2}(1-\Upsilon)\right]\right\} . \quad (87)$$

Also we rewrite the strength of the potential U as

$$U^{-1} \cong \frac{1}{2M\omega_o} - \frac{2\pi\bar{g}_E^2\omega_r^3}{M^2(\omega_r^2-\omega_o^2)^2}\left(1 - \frac{X_u}{32\pi\omega_r^3\omega_o^3}\right) \quad (88)$$

where $X_u = M\omega_o^2(\omega_o^2-\omega_r^2)^2 - 8[\omega_r^2\Upsilon(\omega_o^2-\omega_r^2)^2 + 2\pi\omega_r^4(\omega_r^2-3\omega_o^2)]$. By combining these expressions together, we rewrite the real and imaginary part of the Green's function of Eqs. (85) and (86), respectively, as

$$g'_p(0) \cong -\frac{\bar{g}_E^2\pi\omega_r^3}{2M^2(p^2\omega_o^2+\omega_r^2)^2} \quad (89)$$

and

$$g''_p(0) = \frac{1}{2Mp\omega_o}\left[1 + \frac{\bar{g}_E^2 X_g}{8Mp^2\omega_o^2(p^2\omega_o^2+\omega_r^2)^2}\right] , \quad (90)$$

where $X_g = 4\omega_r^2[\pi\omega_r^2(3p^2\omega_o^2+\omega_r^2) - 2\Upsilon p^2(p^2\omega_o^2+\omega_r^2)^2] + Mp^2\omega_o^2(p^2\omega_o^2+\omega_r^2)^2$. Now, we use Eqs. (88) - (90) and rewrite the simplified phase shift $\delta(p)$ of Eq. (83) as

$$\delta(p) \cong \cot^{-1} p - \frac{\bar{g}_E^2\pi\omega_r^3 X_p}{2Mp(1+p^2)X_\omega} \quad (91)$$

where $X_p = -(\omega_o^2\omega_r^3 + 2\omega_o\omega_r^4 + \omega_r^5) + p^2(2\omega_o^5 + \omega_o^4\omega_r - 4\omega_o^3\omega_r^2 - 3\omega_o^2\omega_r^3 - 8\omega_o\omega_r^4 - 4\omega_r^5) - p^4(16\omega_o^3\omega_r^2 + 8\omega_o^2\omega_r^3) - p^6(8\omega_o^5 + 4\omega_o^4\omega_r)$ and $X_\omega = \omega_o^2(\omega_o+\omega_r)^2(p^2\omega_o^2+\omega_r^2)^2$. Finally, we substitute $\delta(p)$ of Eq. (91) into R_{cav} of Eq. (82) and evaluate the integral to obtain

$$R_{cav} \cong 2 + \frac{\pi\bar{g}_E^2\omega_r^2}{2M\omega_o^2}\frac{X_R}{(\omega_r+\omega_o)^3} , \quad (92)$$

where $X_R = 5\omega_r^3 + 15\omega_r^2\omega_o + 12\omega_r\omega_o^2 - 2\omega_o^3$. Equation (92) yields $R_{cav} = 2$ in the absence of the resonant cavity (i.e., $\bar{g}_E^2 = 0$) as expected.[39]

APPENDIX B: CALCULATION OF L_{cav}

The factor L_{cav} of Eq. (64) may be estimated by determining the bounce-like trajectories $q(\tau)$. The trajectories obey the equation of motion given by

$$-M_e\frac{d^2q(\tau)}{d\tau^2} + \frac{dV_Q(q)}{dq} + 4\pi\bar{g}_E^2\int_{-\infty}^{\infty} d\tau' K(\tau-\tau')q(\tau) = 0 . \quad (93)$$

We rewrite the equation of motion in a convenient form by integrating Eq. (93) by parts and obtain

$$-\frac{M_e}{2}\left(\frac{dq}{d\tau}\right)^2 + V_Q(q) + 4\pi\bar{g}_E^2\int_{-\infty}^{\infty} d\tau' K(\tau-\tau')q(\tau)q(\tau') = 0. \quad (94)$$

Using this result, we write the factor L_{cav} as

$$L_{cav} \approx \frac{M_e}{2}\int d\tau\left(\frac{dq}{d\tau}\right)^2 = \int_{(q_o/2)_-}^{(q_o/2)_+} dq\sqrt{V_Q(q) + 2\pi\bar{g}_E^2\omega_r^2 qQ(\tau)} \quad (95)$$

where $q = q(\tau)$ and

$$Q(\tau) = \int_{-\infty}^{\infty} d\tau' e^{-\omega_r|\tau-\tau'|}q(\tau') . \quad (96)$$

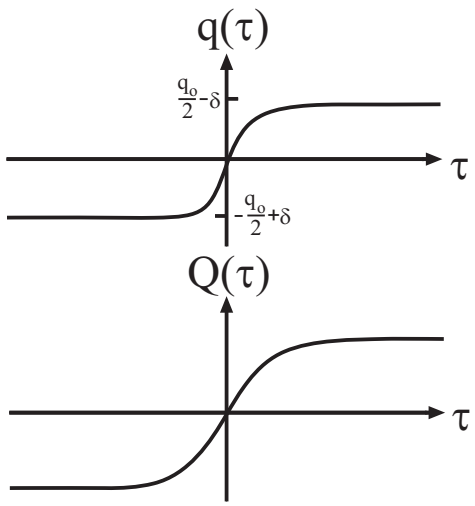

FIG. 15: Similarity between the function $Q(\tau)$ of Eq. (96) and the instanton solution $q(\tau)$ representing the trajectory of the fluxon from one potential minimum to the other via tunneling is illustrated schematically.

Here, the non-local contribution due to resonant cavity is accounted for by $Q(\tau)$. As discussed in Appendix C, the function $Q(\tau)$ is similar to $q(\tau)$. By exploiting this similarity, we expand $Q(\tau)$ in a power series as

$$Q(\tau) = \sum_{n=0}^{\infty} d_{2n+1} q^{2n+1}(\tau) \ , \tag{97}$$

where d_{2n+1} is the expansion coefficients (see Appendix C). The power series expansion for $Q(\tau)$ allows us to evaluate the factor L_{cav} straightforwardly. By using this power series expansion, we evaluate the integral of Eq. (95) in the weak-coupling regime (i.e., $\bar{g}_E^2 \ll 1$) and obtain the factor L_{cav} to the leading order in $\bar{g}_E^2$ as

$$L_{cav} \approx \mathcal{V}_M[A_o + \bar{g}_E^2(B_0 + B_2 q_o^2 + B_4 q_o^4)] \ , \tag{98}$$

where $\mathcal{V}_M = q_o\sqrt{2MV_o}$, $A_o = 1 - q_o^2(2\epsilon b_1/3V_o) - q_o^4(4\epsilon b_2/15V_o)$, $B_0 = -(\epsilon + 8b_3\omega_r^2)/8\epsilon$, $B_2 = [b_1\epsilon + 2(6b_1b_3-1)\omega_r^2 + 2\pi d_1\omega_r^3]/6V_o$, and $B_4 = [b_2\epsilon + 20b_2b_3\omega_r^2 + \epsilon) + 3\pi d_3\omega_r^3]/15V_o$. The frequency independent constants b_i are given by $b_1 = (\cosh\ell - 2)\mathrm{sech}^4(\ell/2)$, $b_2 = (\cosh 2\ell - 26\cosh\ell + 33)/(\cosh\ell + 1)^3$, and $b_3 = (\sinh\ell\tanh\ell)^2/(\cosh 2\ell - 7)$.

APPENDIX C: POWER SERIES EXPANSION OF $Q(\tau)$

The numerically computed function $Q(\tau)$ of Eq. (96) indicates that $Q(\tau)$ is similar to the functional form of the bounce-like trajectory $q(\tau)$. This similarity suggests that $Q(\tau)$ is a scaled function of $q(\tau)$ as shown schematically in Fig. 15. In this case, we may express the function $Q(\tau)$ as a power series in $q(\tau)$ as

$$Q(\tau) = \sum_{n=0}^{\infty} d_{2n+1} q^{2n+1}(\tau) \ , \tag{99}$$

where d_{2n+1} denotes the coefficient for this power series expansion. We compute the coefficients d_{2n+1} by starting with a series expansion of $q(\tau)$ in τ as

$$q(\tau) = \sum_{n=0}^{\infty} a_{2n+1} \tau^{2n+1} \ , \tag{100}$$

noting that the instanton solution $q(\tau)$ is an odd function of τ. Here, the coefficient d_{2n+1} is obtained by following the five steps as discussed below. First, we write the bounce-like trajectory q in the absence of resonant cavity. This trajectory q may be expressed as

$$q = -b_1\tau + b_2 \tanh^{-1}(b_3 \tanh q), \tag{101}$$

where the constants $b_1 = 2\sqrt{\epsilon/M}\coth\ell$, $b_2 = (\cosh 2q_o + \cosh\ell)/\sinh 2q_o$, and $b_3 = \coth q_o$ depend on the parameters ℓ and ϵ. Second, we expand the right hand side of Eq. (101) as a power series in q as

$$q = -b_1\tau + b_2b_3q\left(1 - \frac{1-b_3^2}{3}q^2 + \frac{2-5b_3^2+3b_3^4}{15}q^4 + \cdots\right) . \tag{102}$$

Here, we find the coefficients a_{2n+1} by substituting the series expansion for $q(\tau)$ of Eq. (100) into Eq. (102). The first three coefficients are given by

$$\begin{aligned} a_1 &= \frac{b_1}{b_2b_3 - 1} \ , \\ a_3 &= \frac{b_1^3b_2b_3(1-b_3^2)}{3(b_2b_3-1)^4} \ , \\ a_5 &= \frac{b_1^5b_2b_3(1-b_3^2)[b_2b_3(3-2b_3^2) + (2-3b_3^2)]}{15(b_2b_3-1)^7} \ . \end{aligned}$$

Third, we use Eqs. (26) and (100) to evaluate $Q(\tau)$ of Eq. (96) explicitly as

$$Q(\tau) = \sum_{n=0}^{\infty} a_{2n+1} \int_0^{\infty} d\tau' \ e^{-\omega_r|\tau-\tau'|}\tau'^{2n+1} \ . \tag{103}$$

Fourth, we evaluate the integrals of Eq. (103) and write $Q(\tau)$ in a power series in τ as

$$Q(\tau) \approx \frac{2}{\omega_r}\left[\tau\left(a_1 + \frac{6a_3}{\omega_r^2} + \frac{120a_5}{\omega_r^4}\right) + \tau^3\left(a_3 + \frac{20a_5}{\omega_r^2}\right) + \tau^5 a_5 + \cdots\right] . \tag{104}$$

Finally, we use the power series expansion for $q(\tau)$ of Eq. (100) and rewrite $Q(\tau)$ of Eq. (99) as

$$Q(\tau) = \tau(d_1a_1) + \tau^3(d_1a_3 + d_3a_1^3) + \tau^5(d_1a_5 + 3d_3a_1^2a_3 + d_5a_1^5) + \cdots \tag{105}$$

This series expansion allows us to obtain the expansion coefficients d_{2n+1} by comparing the power series $Q(\tau)$ of Eqs. (104) and (105). The first three expansion coefficients, d_{2n+1}, are the following:

$$d_1 = \frac{2}{\omega_r}\left(1+\frac{6}{\omega_r^2}\frac{a_3}{a_1}+\cdots\right) ,$$

$$d_3 = \frac{4}{\omega_r^3}\left[\left(\frac{10a_5}{a_1^3}-\frac{3a_3^2}{a_1^4}\right)+\frac{60}{\omega_r^4}\left(\frac{7a_7}{a_1^3}-\frac{a_3a_5}{a_1^4}\right)+\cdots\right] ,$$

$$d_5 = \frac{12}{\omega_r^3}\left[\left(\frac{7a_7}{a_1^5}-\frac{11a_3a_5}{a_1^6}+\frac{3a_3^3}{a_1^7}\right)+\cdots\right] .$$

In Sec. V, we use these expansion coefficients to estimate the dimensionless factor L_{cav} and the one-bounce contribution to the action (i.e., $S_{B,1}^{cav}$).

* Present Address: Department of Physics, University of Colorado Denver, P.O. Box 173364, Denver, CO 80217

[2] A. Wallraff, J. Lisenfeld, A. Lukashenko, A. Kemp, M. Fistul, Y. Koval, and A. V. Ustinov, Nature (London) **425**, 155 (2003).

[3] J. Clarke, Nature (London) **425**, 133 (2003); A. Kemp, A. Wallraf, and A. V. Ustinov, Phys. Stat. Sol. B **233**, 472 (2002).

[4] J. H. Kim, R. Dhungana, and K.-S. Park, Phys. Rev. B **73**, 214506 (2006).

[5] P. D. Shaju and V. C. Kuriakos, Physica C **424**, 125 (2005); G. Carapella, F. Russo, R. Latempa, and G. Costabile, Phys. Rev. B **70**, 092502 (2004); V. M. Kaurov and A. B. Kuklov, Phys. Rev. A **71**, 011601(R) (2005).

[6] Y. Nakamura, Y. A. Pashkin, and J. S. Tsai, Nature (London) **398**, 786 (1996); Y. A. Pashkin, T. Yamamoto, O. Astafiev, Y. Nakamura, D. V. Averin, and J. S. Tsai, *ibid.* **421**, 823 (2003).

[7] J. M. Martinis, S. Nam, J. Aumentado, and C. Urbina, Phys. Rev. Lett. **89**, 117901 (2002); Y. Yu, S. Han, X. Chu, S.-I. Chu, and Z. Wang, Science **296**, 889 (2002).

[8] J. R. Friedman, V. Pael, W. Chen, S. K. Tolpygo, and J. E. Lukens, Nature (London) **406**, 43 (2000); C. H. van der Wal, A. C. J. T. Haar, F. K. Wilhelm, R. N. Schouten, C. J. P. M. Harmans, T. P. Orlando, S. Llyod, and J. E. Mooji, Science **290**, 773 (2000); I. Chiorescu, Y. Nakamura, C. J. P. M. Harmans, and J. E. Mooji, *ibid.* **299**, 1896 (2003).

[9] A. N. Price, A. Kemp, D. R. Gulevich, F. V. Kusmartsev and A. V. Ustinov, LANL arXiv:0807.0488v2 [cond-mat].

[10] See for example, G. P. Bermana , A. R. Bishopb, A. A. Chumaka,c, D. Kiniond, and V. I. Tsifrinoviche, LANL arXiv:0912.3791v1 [quant-ph]; F. W. Strauch, S. K. Dutta, H. Paik, T. A. Palomaki, K. Mitra, B. K. Cooper, R. M. Lewis, J. R. Anderson, A. J. Dragt, C. J. Lobb and F. C. Wellstood, IEEE Trans. Appl. Supercond. **17**, 105 (2007); J. Majer, J. M. Chow, J. M. Gambetta, J. Koch, B. R. Johnson, J. A. Schreier, L. Frunzio, D. I. Schuster, A. A. Houck, A. Wallraff, A. Blais, M. H. Devoret, S. Girvin and R. J. Schoelkopf, Nature **449**, 443 (2007).

[11] G. Yi-Bo and L. Chong, Commun. Theor. Phys. **43** 213 (2005); S.-L. Zhu, Z. D. Wang and K. Yang, Phys. Rev. A **68** 034303 (2003); Y. Lui, L. F. Wei, and F. Nori, Phys. Rev. A **72**, 033818 (2005).

[12] E. Almaas and D. Stroud, Phys. Rev. B **65**, 134502 (2002).

[13] I. Tornes and D. Stroud, Phys. Rev. B **71**, 144503 (2005).

[14] Ch. Helm, Ch. Preis, Ch. Walter, and J. Keller, Phys. Rev. B **62**, 6002 (2000); Ch. Helm, Ch. Preis, F. Forsthofer, J. Keller, K. Schlenga, R. Kleiner, and P. Müller, Phys. Rev. Lett. **79**, 737 (1997).

[15] S. Sakai, A. V. Ustinov, H. Kohlstedt, A. Petraglia, and N. F. Pedersen, Phys. Rev. B **50**, 12905 (1994).

[16] J. H. Kim and J. Pokharel, Physica C **348**, 425 (2003).

[17] R. Kleiner, P. Müller, H. Kohlstedt, N. F. Pedersen, and S. Sakai, Phys. Rev. B **50**, 3942 (1994).

[18] A. Davidson and N. F. Pedersen, Appl. Phys. Lett. **60**, 2017 (1992).

[19] A. Irie and G. Oya, Physica C **293**, 249 (1997).

[20] S. Madsen and N. Grønbech-Jensen, Phys. Rev. B **71**, 132506 (2005); N. Grønbech-Jensen, N. F. Pedersen, A. Davidson, and R. D. Parmentier, Phys Rev. B **42**, 6035 (1990).

[21] S. Madsen, G. Filatrella, and N. F. Pedersen, Euro. Phys. J. B **40**, 209 (2004).

[22] A. O. Sboychakov, S. Savel'ev and F. Nori, Phys. Rev B **78**, 134518 (2008).

[23] S. Madsen, N. F. Pedersen, and P. L. Chistiansen, Physica C **468**, 649 (2008).

[24] T. Kato and M. Imada, J. Phys. Soc. Jpn. **65**, 2963 (1996); H. Simanjuntak and L. Gunther, Phys. Rev. B **42**, 930 (1990).

[25] A. Shnirman, E. Ben-Jacob, and B. A. Malomed, Phys. Rev. B **56**, 14677 (1997).

[26] J. H. Kim and K. Moon, Phys. Rev. B **71**, 104524 (2005).

[27] E. G. Maksimov, P. I. Arseyev and N. S. Maslova, Solid State Commun. **111**, 391 (1999).

[28] E.T. Jaynes and F. W. Cummings, Proc. IEEE **51**, 89 (1963).

[29] D. W. McLaughlin and A. C. Scott, Phys. Rev. **A 18**, 1652 (1978).

[30] A. O. Caldeira and A. J. Leggett, Ann. Phys. (NY) **149**, 374 (1983); *ibid.* Phys. Rev. Lett. **81**, 211 (1981).

[31] See for example, A. J. Leggett, S. Chakravarty, A. Dorsey, M. A. P. Fisher, A. Garg and W. Zwerger, Rev. Mod. Phys. **59**, 1 (1987).

[32] J.-L. Gervais, A. Jevicki and B. Sakita, Phys. Rev. D **12**, 1038 (1975).

[33] C. Gorria, P. L. Christiansen, Yu. B. Gaididei, V. Muto, N. F. Pedersen, and M. P. Soerensen, Phys. Rev. B **68**, 035415 (2003); P. Woafo, Phys. Lett. A **302**, 137 (2002).

[34] J. Sethna, Phys. Rev. B **24**, 698 (1981).

[35] J. S. Langer, Ann. Phys. (N.Y.) **41**, 108 (1967); C. G. Callan, Jr. and S. Coleman, Phys. Rev. D **16**, 1762 (1977).

[36] T. Banks, C. M. Bender, and T. T, Wu, Phys. Rev. D **8**, 3346 (1973).

[37] J. H. Kim, I. D. O'Bryant and R. P. Dhungana (unpublished).

[38] H. Grabert, U. Weiss and P. Hanggi, Phys. Rev. Lett. **52**, 2193 (1984).

[39] A. Garg, Am J. Phys. **68**, 430 (2000).

[40] S. Coleman, *Aspects of symmetry* (Cambridge University

Press, Cambridge, 1985) p. 265.
[41] U. Weiss, H. Grabert, P. Hanggi, and P. Riseborough, Phys. Rev. B **35**, 9535 (1989).
[42] P. L. Knight and P. W. Milonni, Phys. Rep. **66**, 21 (1980); Also see, for example, C. C. Gerry and P. L. Knight, *Introductory Quantum Optics* (Cambridge University Press, Cambridge, 2005).
[43] A. Garg, J. Onuchic and V. Ambegaokar, J. Chem. Phys. **83**, 4491 (1987); M. Murao and F. Shibata, J. Phys. Soc. Jpn **64**, 2394 (1995).
[44] J. Major, J. M. Chow, J. M. Gambetta, J. Koch, B. R. Johnson, J. A. Schreie, L. Frunzio, D. I. Schuster, A. A. Houck, A. Wallraff, A. Blais, M. H. Devoret, S. M. Girvin, and R. J. Schoelkopf, Nature **449**, 443 (2007); M. Sillanpaa, J. Park, and R. Simmonds, Nature (London) **449**, 438 (2007); J. M. Fink, R. Bianchetti, M. Baur, M. Göppl, L. Steffen, S. Filipp, P. J. Leek, A. Blais, and A. Wallraf, Phys. Rev. Lett. **103**, 083601 (2009).
[45] M. Tavis and F. W. Cummings, Phys. Rev. **170**, 379 (1968).
[46] S. Hill and W. K. Wootters, Phys. Rev. Lett. **78**, 5022 (1997).